Application of stress test concepts for port infrastructures against natural hazards. The case of Thessaloniki port in Greece.

Kyriazis Pitilakis [a], Sotiris Argyroudis [a,b,*], Stavroula Fotopoulou [a], Stella Karafagka [a], Kalliopi Kakderi [a], Jacopo Selva [c]

[a] *Department of Civil Engineering, Aristotle University, Thessaloniki, Greece*

[b] *Department of Civil & Environmental Engineering, University of Surrey, Guildford, United Kingdom*

[c] *Istituto Nazionale di Geofisica e Vulcanologia, Bologna, Italy*

ABSTRACT

An engineering risk-based methodology for stress testing of critical infrastructures is applied to the port of Thessaloniki in Greece exposed to seismic, geotechnical and tsunami hazards. The methodology workflow consists of four phases: Pre-Assessment, Assessment, Decision and Report phase. In the pre-assessment phase, all the necessary information of the port is archived. The inventory includes the main port components namely buildings, waterfronts, cranes and the electric power supply system. Generic or site-specific fragility models are used for all exposed elements and considered hazards. Risk metrics and objectives are defined related to the functionality of the system and the structural losses. In the first level of the assessment phase, the performance of each component is evaluated using a risk-based approach. Then, a system level probabilistic risk analysis is conducted separately for earthquake and tsunami hazards. A complementary scenario-based risk analysis carried out aiming to investigate the impact of site-specific response and extreme seismic events to the performance of the port. In the Decision phase, the results are compared with predefined objectives to decide whether the infrastructure passes, partly passes or fails the test. Guidelines and strategies to improve the performance and resilience of the port are summarized.

Keywords: critical infrastructure; stress test; probabilistic risk assessment; scenario-based risk assessment; earthquake; liquefaction; tsunami; systemic analysis

1. INTRODUCTION

Critical Infrastructures (CIs) provide the essential services to the society and represent the backbone of the economy, security, and health. Among critical infrastructures, ports provide the necessary services for the maritime passengers and freight transportation. Ports play a crucial role in world economy since around 90% of world trade is carried by the international shipping industry, while seaborne trade volumes surpassed 10 billion tons in 2015 (UNCTAD 2016). Therefore, resilience and continuous operation of ports are interrelated with the international, national and regional growth and development. However, ports are usually located in areas prone to geo- and climatic hazards such as earthquakes, tsunami, liquefaction, overtopping events or erosion. The high vulnerability of port facilities has been revealed in past natural disasters.

*Corresponding Author:
E-mail address: sarg@civil.auth.gr (S. Argyroudis)

Evidence from past earthquakes suggests that most damage to port structures is associated with significant deformation of soft or liquefiable soil deposits. In case of tsunami disasters, in addition to direct damages due to waves, ships, non-anchored equipment or pieces of cargo can be moved or carried away by the tsunami waves, becoming debris that can collide with other structures and cause significant damage. Ports can be seriously affected by the disruption of other infrastructure such as the electric power network, while the cascading and long-term effects may be also very important. A typical example is the port of Kobe in Japan, one of the largest container cargo ports in the world, which suffered major damages during the 1995 M_w6.8 Hyogoken-Nanbu earthquake (NCEER 1995). Although most of the damage had been restored within one year, it is remarkable that three years after the disaster, cargo traffic remained at roughly half of the pre-disaster levels (Chang 2000). The M_w9.0 Tohoku earthquake and tsunami in Japan which caused severe damage to port infrastructure and had a massive economic impact is another characteristic example (TCLEE 2012). The 1999 M_w7.6 Kocaeli earthquake in Turkey, caused heavy damage and significant economic loss to a large number of waterfront structures, utilities, and tanks, indicated that port facilities are particularly susceptible to liquefaction-induced ground deformations (Erdik 2000).

Lessons learned from previous disasters showed that losses had severe consequences on trade and economy, which in several cases exceeded the local or national scale. Although awareness of the risks in the maritime sector is increasing the last years, the port planning to natural hazards is still insufficient. Thus, reliable assessment of the vulnerability and associated risks for port infrastructure is an urgent need of paramount importance. In particular, since we cannot prevent natural disasters, but we can mitigate their impacts, advanced and standardized tools for vulnerability and risk assessment of port infrastructure are required. Such tools will enable the efficient allocation of resources toward more reliable and resilient ports, including risk reduction measures and repair, maintenance and contingency planning by port stakeholders.

So far, numerous studies have analyzed the failure modes and vulnerability of port components exposed to seismic and other hazards (e.g. NIBS 2004; Ichii 2004; Na and Shinozuka 2009; Kakderi and Pitilakis 2010; Kosbab 2010; Berle et al., 2011; Miraei and Jafarian 2013; Pitilakis et al., 2014a; Karafagka et al. 2016). Moreover, probabilistic frameworks have been proposed for the risk and performance assessment of the port infrastructure and maritime transport under seismic hazard, climate extremes or human errors (e.g. Guedes Soares and Teixeira 2001; Pachakis and Kiremidjian 2004; Groen et al. 2006; Werner and Taylor 2004; Shafieezadeh and Burden 2014; Alises et al. 2014; Lam and Lassa 2017). A wide development of methods and models for the resilience and risk assessment of interconnected infrastructures has been seen during the last decades (e.g. Rinaldi et al. 2001; Eusgeld et al. 2011; Filippini and Silva 2014; Ouyang 2014; Nan and Sansavini 2017). The interdependencies are usually classified to physical, cyber, geographical and logical (Rinaldi et al. 2001), while the simulation approaches are grouped to empirical, agent-based, system dynamics based, economic theory based, network-based and other approaches (Ouyang 2014). The studies that specified and modeled interactions between port components and other systems are limited (e.g. Pitilakis et al. 2014b; Hsiesh et al. 2014). Yet, there is a lack of standardized tools for hazard and risk assessment of port infrastructure including low-probability high-consequences (LP-HC) events.

To this regard, a new engineering risk-based multi-level framework for stress tests for non-nuclear CIs of different classes has been recently proposed (Esposito et al. 2017; Stojadinovic et al. 2016) in the framework of the European project STREST (http://www.strest-eu.org). The objective of the present paper is to specify the proposed risk-based multi-level framework for stress tests for the case of port infrastructure and demonstrate its applicability through a pilot study for a real port system.

The port of Thessaloniki, one of the most important ports in Southeast Europe and the largest transit-trade port in Greece, is used as a pilot study. The scope is to demonstrate how the different levels of the methodology are applied to a real port facility focusing to critical components and interactions.

2. STRESS TEST CONCEPTS FOR PORT INFRASTRUCTURE

The proposed methodology aims to quantify the safety and the risk of individual components as well as of whole critical infrastructure with respect to natural events and to compare the behavior of the CI to acceptable values (Esposito et al. 2017; Stojadinovic et al. 2016). It is based on a common taxonomy and rigorous models for the hazard, vulnerability, performance and resilience assessment under different natural hazards. A multi-level methodology is proposed based on the potential consequences of a failure of the CI, the types of hazards, and the available resources for conducting the stress tests. Each Stress Test Level (ST-L) is characterized by a different scope (component or system) and by a different level of risk analysis complexity. In particular, three ST-Ls are introduced: ST-L1, a single-hazard component check; ST-L2, a single-hazard system-wide risk assessment; and ST-L3, a multi-hazard system-wide risk assessment. In order to manage the subjectivity and to quantify the epistemic uncertainty a formalized multiple expert integration process has been developed (Selva et al. 2015) and integrated into the stress test workflow (Esposito et al. 2017). Within this process, several groups of experts with different background knowledge and tasks may be involved. The size of such groups and the complexity of the process depends on the selected ST-Level and the complexity of the system to be modeled.

The key actors involved in the implementation of the stress test are the Project Manager (PM, representing the stakeholder), the Technical Integrator (TI, an analyst coordinating the assessment), the Evaluation Team (ET, one or more experts implementing the assessment following the Technical Integrator guide), the Pool of Experts (PoE, experts provide input to the TI for making the critical decisions along the process) and the Internal Reviewers (IR, one or more experts performing a participatory review). PM, TI, and IR remain independent to guarantee fairness of the stress test outcomes, and formally agree on the final stress test implementation. All actors should interact along the stress test to assure the robustness of the results, considering the potential limitation in the available resources.

The stress test framework is composed of four main phases. First, the goals, the method, the time frame, the total costs of the stress test, and the most appropriate level to apply are defined. Then, the stress test is performed at the component and the system level according to the selected ST-Level. Finally, the stress test outcomes are checked, analyzed and presented to the CI authorities and regulators. A penalty system is defined to acknowledge the limitation of the methods and models used to assess the performance of the CI

and, eventually, penalize the output of the risk assessment. Finally, a grading system is proposed to quantify the outcome of the test and to prescribe the degree of safety improvement required for the next planned stress test. The four phases of the general stress test methodology are named Pre-Assessment, Assessment, Decision and Report phase, which are performed in sequence. Each phase is subdivided into a number of specific steps. The specification for the port infrastructure of these phases and steps are specified in Fig. 1 and in the followings.

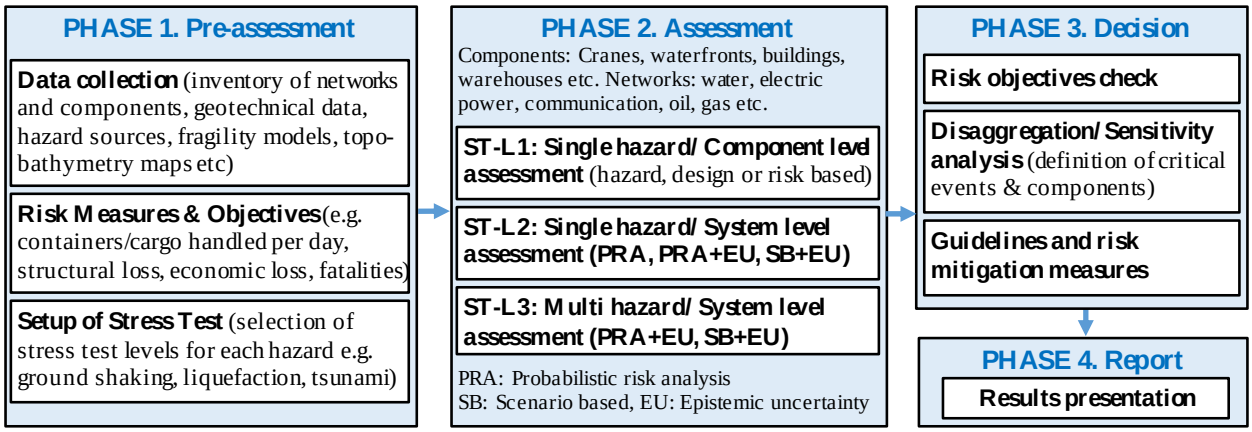

Figure 1. Flowchart of the framework for the stress test application in the port infrastructure (adapted from Esposito et al. 2017)

Phase 1. Pre-Assessment: The PM TI, ET, and IR are selected first. All necessary data and relevant information about hazards (i.e. list of potential natural hazards and sources, available hazard studies and catalogues of events), port infrastructure (i.e. inventories of components and networks inside the port), and previous stress tests that have been conducted in the port or other infrastructure in the area is collected and archived by the TI and ET. The inventory includes data for the port facilities, buildings, quay walls, cranes and networks (e.g. electric power, water, communication, gas and oil networks). The inventory data is associated with: a) the structural characteristics and the typology of the components (e.g. geometry, material, structural type, year of design etc.), which are required for the selection of the fragility functions and the estimation of damage, b) the functional and other characteristics of the components (e.g. handling capacity for cranes, replacement cost and number of occupants for buildings etc.) which are necessary for the estimation of losses. Site and case-specific or generic fragility functions (i.e. Pitilakis et al. 2014a, NIBS 2004) are selected for the vulnerability assessment of the port components to the given hazards (e.g. ground shaking, liquefaction, tsunami, major floods, storms). The PM defines the goals of the analysis, specifying the target performance to be tested (e.g. loss of cargo/containers handling capacity, structural or economic loss etc.) and how to measure this performance through a Performance Indicator (e.g. economic loss, loss in handling capability, etc.). The PM also selects the stress test level(s), as well as, in agreement with the TI, the accuracy of the methods to be adopted according to the available resources and timing for performing the stress test.

Phase 2. Assessment: It comprises two distinctive steps: the component level assessment and the system level assessment (probabilistic or scenario-based). In the first one, the ET checks if each of the port components passes or fails the minimum requirements for its performance against the single hazard using hazard-based, design-based or risk-based assessment approach. For the risk-based approach, the target (acceptable) probability of collapse implied by the code, stakeholders and decision-makers needs should be pre-defined for each component. This level of assessment is obligatory since the design of most components is regulated by design codes, while the data and expertise are available. In the second step, the performance of the port infrastructure is assessed for single or multi-hazards following a probabilistic risk analysis (PRA) and supplementary scenario-based risk analysis (SBRA), for considering phenomena not formally treatable through PRA. Specific interdependencies between networks and components should be considered in the system analysis, while epistemic uncertainties should be treated at high-level stress tests. These steps are not obligatory since they require extensive amount of resources and knowledge. In these steps, the role of experts in the selection of hazards and scenarios, the definition of interdependencies and quantification of epistemic uncertainty, is also critical. However, these steps are highly recommended because only in this way is likely that the most critical components for the reliability of the whole infrastructure can be identified. The choice of implementing/not-implementing this part is therefore accounted for in the penalty system (Esposito et al. 2017).

Phase 3. Decision: The estimated response is compared with predefined acceptable risk criteria in order to assess the performance of the port infrastructure and decide whether it passes, partly passes or fails the test for all possible events and to define how much the safety of the CI should be improved until the next periodical verification. The decision phase also includes disaggregation and/or sensitivity analysis for the identification of the critical components and events, guidelines and strategies to improve the performance and the resilience of the port as a critical facility.

Phase 4. Report: This ultimate phase includes the presentation of the outcome of the stress test by the PM and TI to the Port Authorities. Further details on the three Phases can be found in Esposito et al. (2017).

In the next sections, the different Phases are applied to the port of Thessaloniki, in North Greece, exposed to different seismic related hazards, namely, ground shaking, liquefaction and tsunami. This selection is here made a priori, even if for a more general multi-risk purpose it should derive from a formal prioritization. The risk and safety of the port infrastructure are evaluated at component and system level with respect to the different hazards considering specific interdependencies between networks and components (Pitilakis et al. 2014b). The risk analysis results are compared to predefined acceptable risk objectives. Although several experts have been involved in the case study, including representatives from Thessaloniki Port Authority, the main goal of the present paper is to demonstrate the applicability of the proposed methodology to a real port infrastructure. Therefore, we do not present the specific involvement of the key actors in the different phases focusing on the modeling and the results of each stress test level.

3. PRE-ASSESSMENT PHASE

3.1 Data collection and infrastructure typology

178 The port of Thessaloniki occupies a total space of 1.5 million m^2, includes six piers spreading on a 6200 m
179 long quay and a sea depth down to 12 m, with open and indoors storage areas, suitable for servicing all types
180 of cargo and passenger traffic (Fig. 2). The port also has installations for liquid fuel storage, while is located
181 in proximity to the international natural-gas pipeline and is linked to the national and international road and
182 railway network. In this study, among the different potentially interacting hazards (e.g., seismic, tsunami,
183 floods, storms), only seismic and tsunami hazard have been selected. Similarly, among the different
184 networks and interactions found in the port (i.e. water, waste-water, electric power, communication, oil, gas),
185 only the electric power system was considered in the analysis. These selections were based on the
186 prioritization of all possible hazards and dependencies (Crowley et al. 2016), the feedback from the Port
187 Authority as well as the availability of data and resources for the present pilot study. For the needs of this
188 pilot study, this approach has been considered the only viable, even if it is auspicable in the future to base
189 these decisions on more quantitative approaches (Selva et al. 2015). A GIS database for the port facilities
190 was made available (Kakderi et al. 2010) and further improved by the authors to include the typological
191 characteristics for the components that were considered in the present application: waterfront structures (e.g.
192 gravity retaining structures along the waterfront, quay walls/piers, sheet pile wharves and piers with or
193 without batter piles), cargo handling equipment (e.g. stationary, rail, tire and track mounted gantry and
194 revolver cranes), buildings (e.g. offices, sheds or warehouses of different design codes, structural and
195 material types) and the electric power supply system (e.g. open/ closed type substations with anchored/
196 unanchored components of low, medium and high voltage, over ground/ underground electric power lines)
197 (Fig. 2). The taxonomy defined by Crowley et al. (2016) is used to describe the different typologies of port
198 infrastructure. Waterfront structures include concrete gravity block type quay walls with simple surface
199 foundation and non-anchored components. Cargo handling equipment has non-anchored components without
200 backup power supply. Four gantry cranes are used for container loading-unloading services located in the
201 western part of the 6^{th} pier. The electric power supply to the cranes is provided from the distribution
202 substations that are present inside the port. For the needs of this pilot study and to simplify the analysis,
203 taking also into account the feedback from the Port Authority regarding the most crucial components, it is
204 considered that the electric power lines are non-vulnerable to seismic and tsunami hazards. The substations
205 are classified as low-voltage, with non-anchored components. In total, 85 building and storage facilities are
206 considered in the case study. The majority is reinforced concrete (RC) buildings comprising principally of
207 low-rise (LR) and mid-rise (MR) infilled moment resisting frame (MRF) and dual systems with low (LC) or
208 no (NC) seismic design constructed before 1985. The steel buildings are basically warehouses with one or
209 two floors with or without unreinforced masonry infill walls, while the unreinforced masonry (URM)
210 buildings are old, low-rise and mid-rise structures.
211

Figure 2. Geographical representation of Thessaloniki's port infrastructures considered in the study

Soft alluvial deposits composed mainly of sandy clays and silts, sometimes susceptible to liquefaction, characterize the subsoil conditions of the port. The thickness of these deposits close to the sea reaches 150 m to 180 m. A comprehensive set of in-situ geotechnical tests (e.g. drillings, sampling, SPT and CPT tests), detailed laboratory tests and measurements, as well as geophysical surveys (cross-hole, down-hole, array microtremor measurements) at the port broader area provide all necessary information to perform all kind of site-specific ground response analyses (Anastasiadis et al. 2001; Apostolidis et al. 2004). Complementary geophysical tests including array microtremor measurements have been recently conducted at four different sites inside the port (Pitilakis et al. 2016) using the SPatial Autocorrelation Coefficient–SPAC method (Aki 1957). All available data (Fig. 3) are properly archived. Three representative soil profiles denoted as A, B, and C (Fig. 4) have been defined based on the available data for the site response analyses (section 4.2.2). Their fundamental periods T_o are equal to 1.58 sec, 1.60 sec, and 1.24 sec respectively. Figure 4 presents the variation of the shear wave velocities V_s with depth for the three soil profiles. The variation of the shear modulus G/G_{max} and damping ratio D with shear strain γ at various depths of the soil layers was determined from extended laboratory tests (Pitilakis and Anastasiadis 1998). A topobathymetric model was also produced for the tsunami simulations, based on nautical and topographic maps and satellite images (Cotton et al. 2016; Selva et al. 2016b). The elevation data includes also the buildings and other structures that affect the waves while propagating inland. The resolution of the model is higher in the area of the port.

Figure 3. Location of geotechnical tests and geophysical field measurements in Thessaloniki's port area

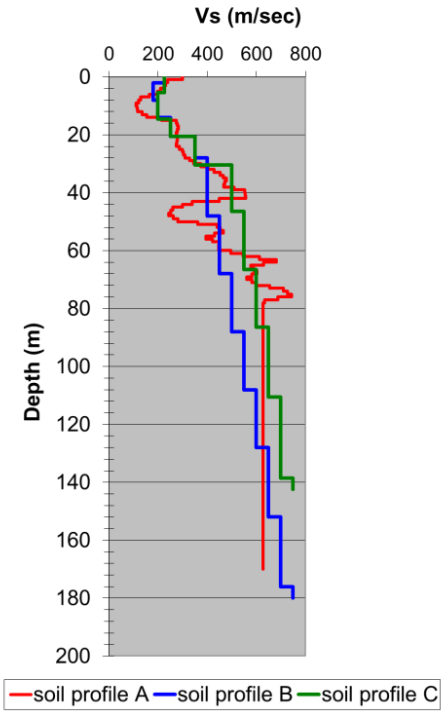

Figure 4. Shear wave velocities (V_s) profiles for sites A, B, and C

231

232 **3.2 Fragility models**

233 Risk and safety evaluation of a port infrastructure presupposes the reliable vulnerability assessment of port
234 components. The vulnerability is commonly evaluated through fragility and/or vulnerability functions which
235 enable to assess the expected damage and loss in each typology of buildings or infrastructure for each given
236 hazard. While the evaluation of the seismic vulnerability has received over the past years a significant

attention (e.g. Calvi et al. 2006; Pitilakis et al. 2014a), the models for the vulnerability assessment related to other hazards (e.g. tsunami, floods, landslides etc.) is still limited (e.g. Fotopoulou and Pitilakis 2013). Therefore there is a clear need to expand the vulnerability and risk assessment methods to other hazards.

In this study, the vulnerability is assessed at the component level (i.e. buildings, waterfront structures, cranes etc.) for the different considered hazards through fragility functions, which provide the probability of exceeding predefined damage states (DS) for given level of hazard intensity. The latter is described by the peak ground acceleration (PGA), permanent ground displacement (PGD) and inundation depth for the ground shaking, liquefaction and tsunami hazards respectively (Table 1). The fragility functions used to assess the damages due to liquefaction are generic (NIBS 2004), while the models used for ground shaking are either site-specific (UPGRADE 2015) or generic (NIBS 2004; Kappos et al. 2003; 2006; SRM-LIFE 2007).

In particular, new seismic fragility curves have been developed for typical quay walls and gantry cranes of the port subjected to ground shaking based on dynamic numerical analyses (UPGRADE 2015). The model included the quay wall blocks, the surrounding soil and the embankment, as well as concentrated gravity loads on the position of container crane legs and a uniform operational load on the embankment (Kourkoulis et al. 2014). Twelve seismic motions were selected in the analyses to account for seismic scenarios of moderate and high seismicity scaled up to different amplitudes (up to ± 0.3g) and applied at the model base through viscous dampers. Then, for each seismic analysis, the engineering demand parameter (EDP) was estimated. In particular, the ratio of the residual displacement (towards the sea) at the top of the wall (u_x) to the height of the quay wall (H) was considered as EDP (u_x/H) for the quay wall, while the resultant (horizontal and vertical) residual differential displacement of the crane legs (d_u) was taken as EDP for the crane. Lognormal distribution functions were established as a function of the peak ground acceleration (PGA) at free field conditions to represent the fragility curves for predefined damage states (according to PIANC 2001 and NIBS 2004 for the quay wall and the crane respectively). Fig. 5 illustrates the fragility curves and its parameters (i.e. median m and log- standard deviation beta) for the quay walls and the cranes.

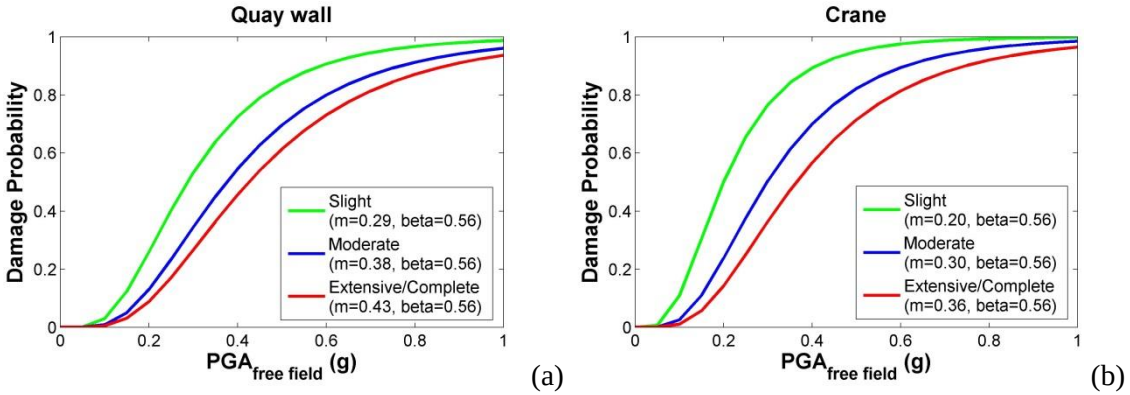

Figure 5. Fragility curves for the quay walls (a) and the cranes (b) for ground shaking

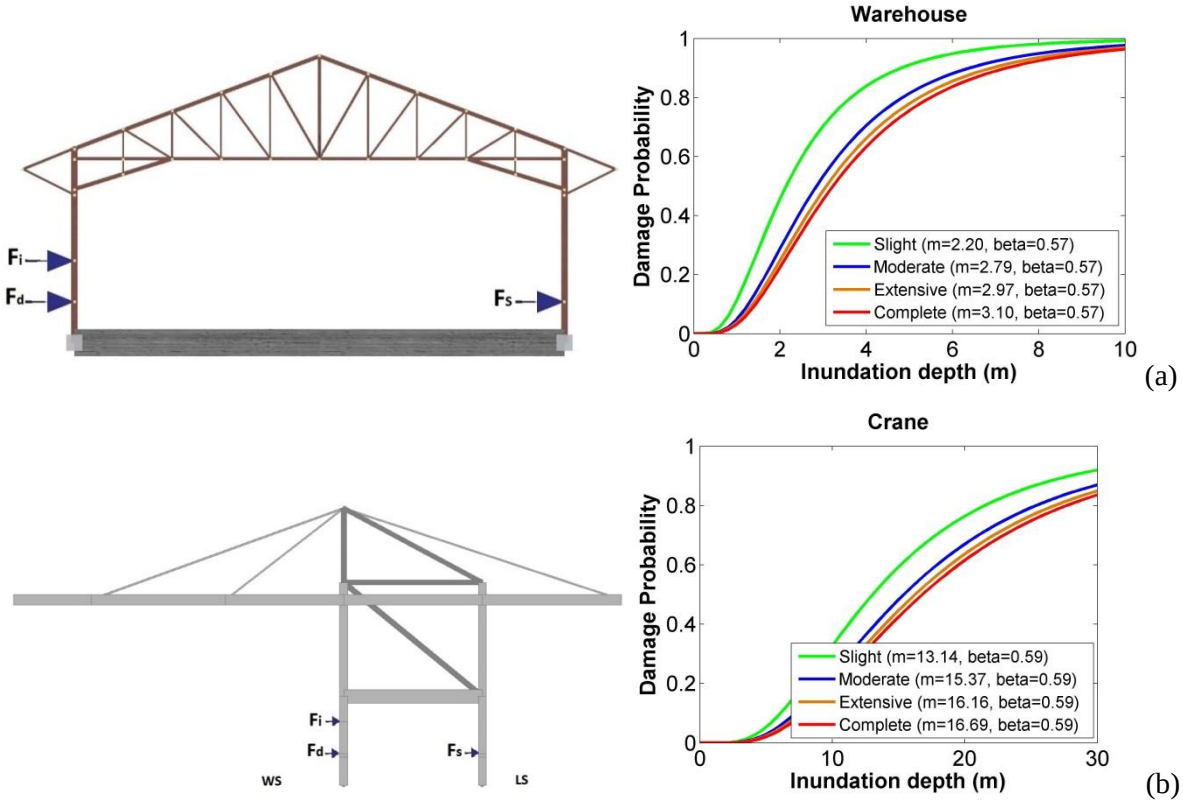

Figure 6. Tsunami structural models and fragility curves for the warehouse (a) and the cranes (b)

Analytical tsunami fragility curves as a function of inundation depth have been developed for representative typologies of the RC buildings, warehouses and gantry cranes (Karafagka et al. 2016; Salzano et al. 2015) while, for simplicity reasons, the waterfront structures are considered as non-vulnerable to tsunami forces. An extensive numerical parametric investigation has been performed based on nonlinear static analyses of typical port structures. Different combinations of statically applied tsunami loads based on FEMA (2008) recommendations have been considered for gradually increasing tsunami inundation depths. Afterward, the structure's response in terms of material strain (i.e. the EDP) for the different statically applied tsunami loads was estimated. For the development of fragility curves, a relationship between the numerically calculated material strain (i.e. the EDP) and the gradually increasing inundation depths (i.e. the IM) was established through nonlinear regression analysis. Indicatively, the structural models and tsunami fragility curves for warehouses and cranes are presented in Fig. 6.

The damage states are correlated with the functionality of each component in order to perform the risk assessment at the system level. The following assumptions were adopted for all types of hazards: (i) the waterfront-pier (berth) is functional if damage is lower than moderate, (ii) the crane is functional if damage is lower than moderate and there is electric power supply (i.e. when the physical damages of the substations are lower than moderate), (iii) the berth is functional if the waterfront and at least one crane are functional.

Table 1. Fragility functions used in the risk analyses

Hazard	Component	Intensity measure	Reference
Ground shaking	RC and URM buildings	PGA	Kappos et al. (2003; 2006)
	Steel buildings		HAZUS (NIBS 2004)
	Waterfront structures		UPGRADE (2015) - Fig. 5
	Cranes/cargo handling equipment		
	Electric power substations (distribution, transmission)		HAZUS (NIBS 2004), SRM-LIFE (2003-2007)
Liquefaction	Buildings/ Housed electric power substations (all considered typologies)	PGD	HAZUS (NIBS 2004)
	Waterfront structures		
	Cranes/cargo handling equipment		
Tsunami	RC Buildings/ Electric power substations	Inundation depth	Karafagka et al. (2016), Salzano et al. (2015) - Fig. 6
	Warehouses (steel and URM buildings)		
	Cranes/cargo handling equipment		

3.3 Set-up of the Stress Test

In order to demonstrate the applicability of the proposed framework, the port infrastructure of Thessaloniki is subjected to seismic and tsunami hazards ST-L1 and ST-L2. First, a component level risk-based assessment of the key components is carried out for seismic and tsunami hazards (ST-L1). Then, a probabilistic risk analysis is undertaken at the system level considering separately seismic and tsunami hazards (ST-L2). Complementary to the PRA, a scenario-based system-wide risk assessment is conducted to further investigate extreme seismic events including liquefaction and site-specific response. Different approaches are considered to account for the scenario-based single-risk (L2) (i.e. due to ground shaking) and multi-risk (L3) (i.e. due to ground shaking and liquefaction) assessments at the system level. Two return periods are considered corresponding to a normal (i.e. 475 years) and LP-HC (i.e. 4975) event scenarios.

3.4 Definition of risk metrics and objectives

In the Pre-Assessment phase, specific risk metrics and objectives are defined related to the structural losses at the component level and the functionality of the port at the system level. For level 1 assessment, the annual probability of structural collapse is taken as the risk measure, and the required objective is sought by reference to European design norms. In particular, the reference target (acceptable) probability of collapse is

304 set equal to $1.0 \cdot 10^{-5}$ based on the existing practice (e.g. Lazar and Dolšek 2013; Silva et al. 2014a) and is
305 properly modified based on EC8 prescriptions to account for the importance factor γ_I of the structure.
306 For level 2 assessment, two terminals (container, bulk cargo) are assumed and thus the system performance
307 is measured through the total number of containers handled (loaded and unloaded) per day (TCoH), in
308 Twenty-foot Equivalent Units (TEU), and the total cargo handled (loaded and unloaded) per day (TCaH), in
309 tons. Risk measures related to structural and economic losses of the buildings are also set for the tsunami
310 case and the scenario-based assessment. More specifically, for the tsunami probabilistic risk assessment, the
311 performance of the port buildings is assessed through the percentage of buildings being in the complete
312 damage state. For the scenario-based assessment, a structural damage index d_m weighted with respect to the
313 built area is evaluated to quantify the structural losses as the ratio of the cost of repair to the cost of
314 replacement. The risk objectives correspond to the boundaries of the grading system in the proposed
315 framework.
316 The CI passes the stress test if is classified into grade AA (negligible risk) or A (risk being as low as
317 reasonably practicable, ALARP). The CI partly passes the stress test if it receives grade B (possibly
318 unjustifiable risk), while it fails the stress test if it is classified into grade C (intolerable risk).
319 Since no regulatory boundaries (AA-A, A-B, and B-C) exist presently for port facilities, to demonstrate the
320 application of the proposed methodology, indicative continuous boundaries, i.e. straight lines on the
321 logarithmic performance curve, were defined for the probabilistic system-wide risk assessment in terms of
322 the annual probability for 100% loss, assuming a logarithmic slope equal to 1 (neutral risk), (i.e., B-C:
323 $4.5 \cdot 10^{-3}$, A-B: $2.0 \cdot 10^{-3}$, AA-A: $7.5 \cdot 10^{-4}$). For the scenario-based assessment, scalar boundaries in terms of the
324 expected performance loss (%) are assigned for the normal (B-C: 50, A-B: 30, AA-A: 10) and the extreme
325 (B-C: 70, A-B: 50, AA-A: 30) event scenarios based on general judgment criteria. It is worth noting that, for
326 the system level assessment (ST-L2), risk objectives related to the structural and economic losses of the
327 buildings were not defined since the buildings were considered separately in the probabilistic tsunami and
328 the scenario-based assessments as their performance was not expected to significantly affect the performance
329 of the port system.
330
331 **4. ASSESSMENT PHASE**
332 **4.1 Component level assessment**
333 The aim is to check each component of the port independently for earthquake and tsunami hazards in order
334 to show whether the component passes or fails the pre-defined minimum requirements for its performance
335 implied by the current codes. A risk-based assessment is performed using the hazard function at the location
336 of the component and the fragility function of the component. These two functions are convolved in risk
337 integral in order to obtain the probability of exceedance of a designated limit state in a period of time (P_f).
338 This probability is estimated on the basis of closed-form risk equation (Fajfar and Dolšek 2012) as follows:

339 $$P_f = H(\overline{IM}) \exp(0.5 k^2 \beta^2) \quad (1)$$

where $\overline{IM}$ and β are the median and log-standard deviation values respectively of the fragility function (see Table 1), H(IM) is the hazard function and k is the logarithmic slope of the hazard function idealized in the following form:

$$H(IM) = k_o \cdot IM^{-k} \quad (2)$$

where k_o is a constant that depends on the seismicity of the site. Proper k and k_o can be obtained by fitting the actual hazard curve provided that the entire hazard function or at least two points from the hazard function are available. For the seismic case (i.e. ground shaking), k and k_o were computed from the hazard curve corresponding to return periods equal to 475 and 4975 years for the normal and the extreme event respectively based on the site-specific equivalent linear response analyses carried out for three representative soil profiles A, B and C (scenario-based assessment), which generally leads to higher PGA values compared to the corresponding nonlinear response analyses that take also into account the possibility of liquefaction (e.g. Fig. 7a). For the tsunami case, at least two points of the mean hazard function estimated from probabilistic tsunami hazard assessment at various locations in the port area (Pitilakis et al. 2016; Selva et al. 2016b) were used to estimate these parameters (e.g. Fig. 7b). The target (acceptable) probability of exceedance of a designated limit state for a period of time implied by the code, stakeholders and decision makers (P_t) also has to be defined for each component and different limit states. In this application, the target probability of exceedance of the collapse damage state is only provided. This probability is set equal to $1.0 \cdot 10^{-5}$ based on the existing practice (e.g. Lazar and Dolšek 2013; Silva et al. 2014) corresponding to an acceptable probability equal to 0.05% in 50 years and is properly modified based on EC8 prescriptions to account for the importance factor γ_I of the structure based on the following equation:

$$\gamma_I = (P_L / P_{LR})^{(-1/k)} \quad (3)$$

where P_{LR} the reference acceptable probability of collapse (equal to 10^{-5}) and P_L the modified acceptable probability of collapse to account for the importance of the structure (γ_I). In particular, to check whether or not the component is safe against collapse, the finally computed target probability (P_t) is compared with the corresponding probability of exceeding the ultimate damage state (P_f).

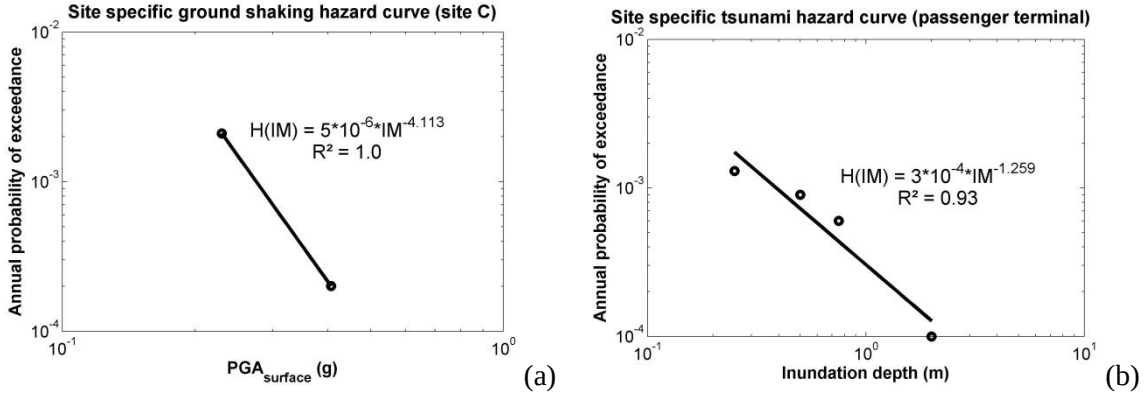

Figure 7. Site-specific hazard curves for ground shaking (a) and tsunami (b)

As an example, the proposed performance assessment approach is applied here to a critical building of the port, the passenger terminal, which is a low-rise infilled dual system (γ_I=1.2). The probability of exceeding the ultimate damage state (P_f), which in this study corresponds to the collapse damage state, is computed and compared with the target probability of collapse (P_t) for both earthquake and tsunami hazards. The hazard function at the location of the structure is estimated as 10^{-5} and $1.7 \cdot 10^{-4}$ for the seismic (see Fig. 7a and Equation 2) and tsunami (see Fig. 7b and Equation 2) case respectively, while the corresponding probabilities of collapse (P_f) are finally computed equal to $1.4 \cdot 10^{-3}$ and $2.0 \cdot 10^{-4}$. These probabilities are higher than the target (acceptable) probability of collapse (P_t) estimated equal to $4.7 \cdot 10^{-6}$ and $7.9 \cdot 10^{-6}$ for the seismic and tsunami case respectively, indicating that the structure is not safe against exceedance of the collapse limit state due to the considered hazards. Tables 2 and 3 present a summary of the component level check for all buildings and infrastructures for the seismic and tsunami case providing a general assessment of the performance and resilience of the port. It is shown that most of the considered port components do not pass the safety test against collapse for both earthquake and tsunami hazards.

Table 2. Earthquake hazard component check

Components		Soil profile	Hazard parameters		Fragility parameter		P_f	P_t	Safety test
			k	k_o	Median PGA (g)	β			
RC buildings	MRF LR-LC infilled	A	2.50	10^{-5}	0.41	0.73	$4.9 \cdot 10^{-4}$	$6.3 \cdot 10^{-6}$	Not safe
		B	3.94	$5.0 \cdot 10^{-6}$			$1.0 \cdot 10^{-2}$	$4.9 \cdot 10^{-6}$	Not safe
		C	4.11	$5.0 \cdot 10^{-6}$			$1.8 \cdot 10^{-2}$	$4.7 \cdot 10^{-6}$	Not safe
	MRF MR- LC infilled	C	4.11	$5.0 \cdot 10^{-6}$	0.26	0.61	$2.8 \cdot 10^{-2}$	$4.7 \cdot 10^{-6}$	Not safe
	MRF HR-LC infilled	A	2.50	10^{-5}	0.55	0.63	$1.5 \cdot 10^{-4}$	$6.3 \cdot 10^{-6}$	Not safe
	dual LR-LC infilled	A	2.50	10^{-5}	0.85	0.76	$9.3 \cdot 10^{-5}$	$6.3 \cdot 10^{-6}$	Not safe
		B	3.94	$5.0 \cdot 10^{-6}$			$8.8 \cdot 10^{-4}$	$4.9 \cdot 10^{-6}$	Not safe
		C	4.11	$5.0 \cdot 10^{-6}$			$1.4 \cdot 10^{-3}$	$4.7 \cdot 10^{-6}$	Not safe
URM buildings	LR	C	4.11	$5.0 \cdot 10^{-6}$	0.51	0.39	$2.9 \cdot 10^{-4}$	$4.7 \cdot 10^{-6}$	Not safe
	MR	A	2.50	10^{-5}	0.23	0.60	$1.2 \cdot 10^{-3}$	$6.3 \cdot 10^{-6}$	Not safe
		C	4.11	$5.0 \cdot 10^{-6}$			$4.4 \cdot 10^{-2}$	$4.7 \cdot 10^{-6}$	Not safe
Steel buildings		A	2.50	10^{-5}	0.45	0.64	$2.7 \cdot 10^{-4}$	$6.3 \cdot 10^{-6}$	Not safe
		B	3.94	$5.0 \cdot 10^{-6}$			$2.8 \cdot 10^{-3}$	$4.9 \cdot 10^{-6}$	Not safe
		C	4.11	$5.0 \cdot 10^{-6}$			$4.3 \cdot 10^{-3}$	$4.7 \cdot 10^{-6}$	Not safe
Distribution substations		A	2.50	10^{-5}	0.74	0.40	$3.5 \cdot 10^{-5}$	$6.3 \cdot 10^{-6}$	Not safe
		B	3.94	$5.0 \cdot 10^{-6}$			$5.7 \cdot 10^{-5}$	$4.9 \cdot 10^{-6}$	Not safe
		C	4.11	$5.0 \cdot 10^{-6}$			$6.7 \cdot 10^{-5}$	$4.7 \cdot 10^{-6}$	Not safe
Quay walls		A	2.50	10^{-5}	0.29	0.56	$2.2 \cdot 10^{-4}$	$6.3 \cdot 10^{-6}$	Not safe
		B	3.94	$5.0 \cdot 10^{-6}$			$1.6 \cdot 10^{-3}$	$4.9 \cdot 10^{-6}$	Not safe
		C	4.11	$5.0 \cdot 10^{-6}$			$2.3 \cdot 10^{-3}$	$4.7 \cdot 10^{-6}$	Not safe
Cranes		A	2.50	10^{-5}	0.36	0.56	$3.4 \cdot 10^{-4}$	$6.3 \cdot 10^{-6}$	Not safe
		B	3.93	$5.0 \cdot 10^{-6}$			$3.2 \cdot 10^{-3}$	$4.9 \cdot 10^{-6}$	Not safe

Table 3. Tsunami hazard component check

Components		Hazard ID	Hazard parameters		Fragility parameter		P_f	P_t	Safety test
			k	k_o	Median h (m)	β			
RC buildings	MRF LR-LC infilled	56	1.26	$3.0\cdot10^{-4}$	2.33	0.37	$1.2\cdot10^{-4}$	$7.9\cdot10^{-6}$	Not safe
		59-60	2.96	$2.4\cdot10^{-3}$			$3.6\cdot10^{-4}$	$5.8\cdot10^{-6}$	Not safe
	MRF MR-LC infilled	45,48, 52	0.87	10^{-4}	3.74	0.40	$3.4\cdot10^{-5}$	$8.5\cdot10^{-6}$	Not safe
		49	0.77	10^{-4}			$3.8\cdot10^{-5}$	$8.7\cdot10^{-6}$	Not safe
		50	0.39	10^{-4}			$6.1\cdot10^{-5}$	$9.3\cdot10^{-6}$	Not safe
	MRF HR-LC infilled	31-35, 37	1.29	$4.0\cdot10^{-4}$	6.19	0.35	$4.3\cdot10^{-5}$	$7.9\cdot10^{-6}$	Not safe
		36	0.97	10^{-4}			$1.8\cdot10^{-5}$	$8.4\cdot10^{-6}$	Not safe
	dual LR-LC infilled	38,43	0.87	10^{-4}	1.57	0.44	$7.3\cdot10^{-5}$	$8.5\cdot10^{-6}$	Not safe
		39	0.43	10^{-4}			$8.4\cdot10^{-5}$	$9.2\cdot10^{-6}$	Not safe
		40	0.61	10^{-4}			$7.9\cdot10^{-5}$	$8.9\cdot10^{-6}$	Not safe
		41	0.76	10^{-4}			$7.5\cdot10^{-5}$	$8.7\cdot10^{-6}$	Not safe
		53	0.97	10^{-4}			$7.1\cdot10^{-5}$	$8.4\cdot10^{-6}$	Not safe
		54	0.99	10^{-4}			$7.1\cdot10^{-5}$	$8.4\cdot10^{-6}$	Not safe
		55	2.14	$9.0\cdot10^{-4}$			$5.4\cdot10^{-4}$	$6.8\cdot10^{-6}$	Not safe
		56	1.26	$3.0\cdot10^{-4}$			$2.0\cdot10^{-4}$	$7.9\cdot10^{-6}$	Not safe
		57	1.29	$4.0\cdot10^{-4}$			$2.6\cdot10^{-4}$	$7.9\cdot10^{-6}$	Not safe
		58-60	2.96	$2.4\cdot10^{-3}$			$1.5\cdot10^{-3}$	$5.8\cdot10^{-6}$	Not safe
		61	1.20	$2.0\cdot10^{-4}$			$1.3\cdot10^{-4}$	$8.0\cdot10^{-6}$	Not safe
		62	0.97	10^{-4}			$7.1\cdot10^{-5}$	$8.4\cdot10^{-6}$	Not safe
		64	1.31	$2.0\cdot10^{-4}$			$1.3\cdot10^{-4}$	$7.9\cdot10^{-6}$	Not safe
		69	1.84	$5.0\cdot10^{-4}$			$3.0\cdot10^{-4}$	$7.2\cdot10^{-6}$	Not safe
Warehouses		63	1.93	$5.0\cdot10^{-4}$	3.10	0.57	$1.0\cdot10^{-4}$	$7.0\cdot10^{-6}$	Not safe
		65	1.28	$2.0\cdot10^{-4}$			$6.1\cdot10^{-5}$	$7.9\cdot10^{-6}$	Not safe
		68	2.96	$2.4\cdot10^{-3}$			$3.5\cdot10^{-4}$	$5.8\cdot10^{-6}$	Not safe
		70	0.68	10^{-4}			$2.1\cdot10^{-4}$	$8.8\cdot10^{-6}$	Not safe
Distribution substations		19, 21	0.97	10^{-4}	2.33	0.37	$4.7\cdot10^{-5}$	$8.4\cdot10^{-6}$	Not safe
		38, 43-44	0.87	10^{-4}			$5.0\cdot10^{-5}$	$8.5\cdot10^{-6}$	Not safe
		64	1.31	$2.0\cdot10^{-4}$			$7.4\cdot10^{-5}$	$7.9\cdot10^{-6}$	Not safe
		61	1.20	$2.0\cdot10^{-4}$			$8.0\cdot10^{-5}$	$8.0\cdot10^{-6}$	Not safe
Cranes		12-17, 19	0.97	10^{-4}	16.69	0.59	$7.8\cdot10^{-6}$	$8.4\cdot10^{-6}$	Safe
		18	1.25	$2.0\cdot10^{-4}$			$7.7\cdot10^{-6}$	$8.0\cdot10^{-6}$	Safe
		22	0.68	10^{-4}			$1.6\cdot10^{-5}$	$8.8\cdot10^{-6}$	Not safe
		23	1.25	$2.0\cdot10^{-4}$			$7.8\cdot10^{-6}$	$8.0\cdot10^{-6}$	Safe
		25	1.21	$2.0\cdot10^{-4}$			$8.5\cdot10^{-6}$	$8.0\cdot10^{-6}$	Not safe
		27	1.26	$3.0\cdot10^{-4}$			$1.2\cdot10^{-5}$	$8.0\cdot10^{-6}$	Not safe
		29	2.31	$1.1\cdot10^{-3}$			$4.2\cdot10^{-6}$	$6.6\cdot10^{-6}$	Safe

4.2 System level assessment

4.2.1 Probabilistic risk assessment (PRA)

The system-wide probabilistic risk assessment is performed separately for ground shaking, including liquefaction, and tsunami hazard, following the methodology developed by Pitilakis et al. (2014b) and extended by Kakderi et al. (2015). The objective is to evaluate the probability or mean annual frequency (MAF) of events with the corresponding loss in the performance of the port operations. The analysis is based on an object-oriented paradigm where the system is described through a set of classes, characterized in terms

of attributes and methods, interacting with each other. The physical model starts from a pre-defined taxonomy and requires: (i) a description of the functioning of the system (intra-dependencies) under undisturbed and disturbed conditions (i.e., in the damaged state following an event); (ii) a model for the physical and functional damageability of each component (fragility functions); (iii) identification of all dependencies between systems (inter-dependencies); and (iv) definition of adequate Performance Indicators (PIs) for components and the system as a whole, which represent the risk metrics defined in section 3.4. The computational modules include the modeling of hazard events and intensity parameters (hazard class), physical damages of components and performance of the system (network class), and specific interactions among systems (interdependency models). For the application at hand, the direct physical dependencies including the functional damage propagation between the main port components are considered based on the prioritization of all possible dependencies within the port infrastructure (Crowley et al. 2016). A Monte Carlo simulation is carried out sampling events and corresponding damages for the given hazard. The exceedance probability of different levels of performance loss is assessed for the system under the effect of any possible event, and the performance curve is produced, which is equivalent of risk curves for non-systemic probabilistic assessments in single (e.g. PEER formula, Cornell and Krawinkler 2000) and/or multi-risk (e.g. Selva 2013) analysis.

In the present application, the systemic analysis concerns the container and bulk cargo movements affected by the performance of the piers, berths, waterfront and container/cargo handling equipment (cranes) while the interdependency considered is between the cargo handling equipment and the Electric Power Network (EPN) supplying to cranes. The capacity of berths is related to the capacity of cranes (lifts per hour/tons per hour). The functionality state of each component and the whole port system is assessed based on the computed physical damage, taking also into account system inter- and intra-dependencies. Regarding the analysis of the interdependencies it is assumed that if a crane node is not fed by the reference EPN node (i.e. electric supply station) with power and the crane does not have a backup supply, then the crane itself is considered out of service. The functionality of the demand node is based on EPN connectivity analysis as described in Pitilakis et al. (2014b).

Risk assessment for ground shaking

The seismic hazard model provides the means for: (i) sampling events in terms of location (epicenter), magnitude and faulting type according to the seismicity of the study region and (ii) maps of sampled correlated seismic intensities at the sites of the vulnerable components in the infrastructure (Weatherill et al. 2014). When the fragility of components is expressed with different IMs, the model assesses them consistently. Five seismic zones with M_{min}=5.5 and M_{max}=7.5 are selected based on the results of SHARE European research project (Giardini et al. 2013) while the ground motion prediction equation (GMPE) of Akkar and Bommer (2010) is used to estimate the outcrop ground motion parameters. Seismic events are sampled for the seismic zones affecting the port area through a Monte Carlo simulation (10,000 runs). The spatial variability is modeled using the correlation models provided by Jayaram and Baker (2009). For each site of a regular grid of points discretizing the study area, the averages of primary IM (PGA) from the

specified GMPE were calculated, and the residual was sampled from a random field of spatially correlated Gaussian variables according to the spatial correlation model. The primary IM is then retrieved at vulnerable sites by distance-based interpolation and finally, the local IM is sampled conditionally on primary IM. Fig. 8 shows an example map with the primary IM (PGA at rock) computed at points of a regular grid, for a sampled event corresponding to a return period of 500 years, modeling the spatial variability of the ground motion. To scale the hazard to the site condition the amplification factors proposed in EC8 (EN 1998-1 2004) are used in accordance with the site classes that were defined in the study area. HAZUS (NIBS, 2004) and the modeling procedure by Weatherill et al. (2014) are applied to estimate the permanent ground displacements (PGDs) due to liquefaction.

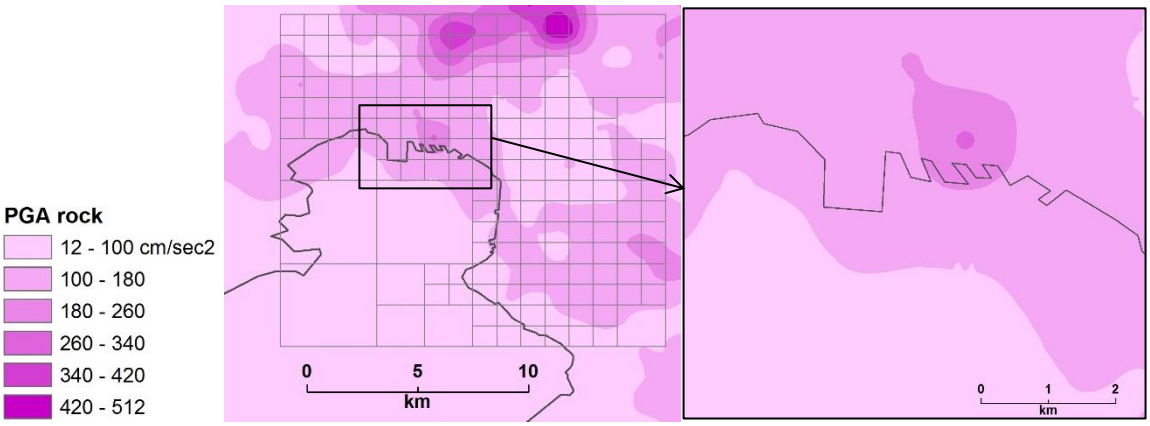

Figure 8. Example of shake map in terms of PGA on rock for one event (M =5.8, R =20 km NNE of the port)

The PIs of the port system for both the container and cargo terminal are evaluated for each simulation of the Monte Carlo analysis based on the damages and corresponding functionality states of each component and considering the interdependencies between components. The final computed PIs are normalized to the value referring to normal (non-seismic) conditions (P_{max}) assuming that all cranes are working at their full capacity 24 hours per day while the performance loss is defined as $1\text{-}PI/PI_{max}$. Fig. 9 shows the MAF of exceedance curves, that is, the "performance curves" for TCoH and TCaH. For performance loss values below 0.4 (i.e. 40% loss), TCaH yields higher values of exceedance frequency, while for performance loss over 0.4, TCoH yields higher values of exceedance frequency. It is also noted that, regardless of the performance loss values, the exceedance frequency for TCoH remains almost constant with a small reduction for higher performance loss values. On the contrary, the values of exceedance frequency for TCaH are abruptly reduced for higher performance loss values. This is related to the larger number of cranes used for cargo handling (34) compared to those used for the containers (4).

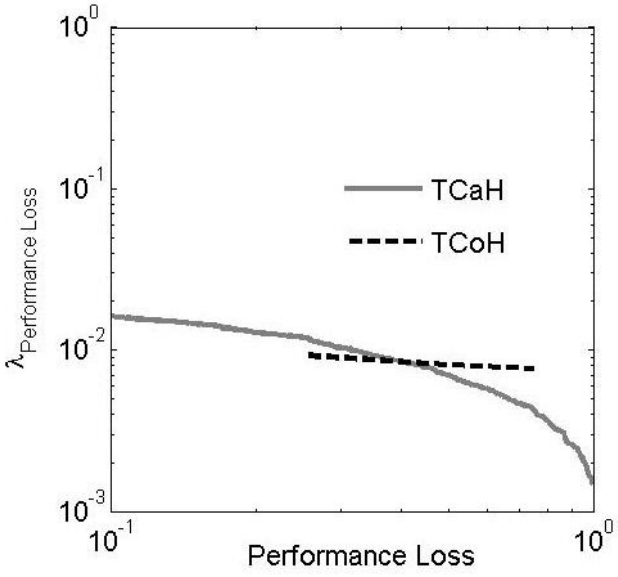

458

459 **Figure 9. Mean annual frequency (MAF) of exceedance values for the normalized performance loss of**
460 **the container terminal (TCoH) and the bulk cargo terminal (TCaH) for the seismic hazard case**
461

462 *Risk assessment for tsunami*

463 A Seismic Probabilistic Tsunami Hazard Analysis (SPTHA) was performed considering tsunamis generated
464 by co-seismic seafloor displacements due to earthquakes (e.g., Davies et al. 2018, Grezio et al. 2017), based
465 on inundation simulation of the Thessaloniki area (Selva et al. 2016b). A very large number of numerical
466 simulations of tsunami generation, propagation and inundation on high-resolution topo-bathymetric models
467 are in principle required, in order to give a robust evaluation of SPTHA at a local site. To reduce the
468 computational cost, while keeping results stable and consistent with respect to explore the full variability of
469 the sources, a method has been developed to approach the uncertainty in SPTHA (Selva et al. 2016a; 2016b),
470 based on four steps: 1) a full exploration of the aleatory uncertainty through an Event Tree (ET, Lorito et al.
471 2015; Selva et al. 2016a) that accounts for all available sources of information (e.g., Basili et al. 2013); 2) the
472 propagation of all potential sources till off-shore (Molinari et al. 2016); 3) a multi-stage filtering procedure
473 based on Cluster Analysis on the results off-shore in order to define a sub-set of "representative" events
474 which approximate the hazard in the target area, in order to enable the inundation modeling (Lorito et al.
475 2015; Selva et al. 2016b); 4) the quantification of the epistemic uncertainty through Ensemble modeling
476 based on (weighted) alternative implementations of steps 1 to 3 (Marzocchi et al. 2015; Selva et al. 2016a).
477 For Thessaloniki port (Selva et al. 2016b), at steps 1 and 2, we considered a regional SPTHA which accounts
478 for all the potential seismic sources from the Mediterranean Sea ($>10^7$ sources), implementing a large
479 number of alternative models to explore the epistemic uncertainty ($>10^5$). Then, the 2-layer filtering
480 procedure has been applied, obtaining 253 representative scenarios which may be modeled to approximate
481 the total hazard (Lorito et al. 2015; Selva et al. 2016b). The numerical simulations were performed using a
482 non-linear shallow-water multi-GPU code (HySEA, Gonzalez Vida et al. 2015), using 4-level nested
483 bathymetric grids with refinement ratio equal to 4 and increasing resolution from 0.4 arc-min (~740 m) to 0.1
484 arc-min (~185 m) to 0.025 arc-min (~46 m) to 0.00625 arc-min (~11 m). The results have been input to an

Ensemble model, in order to quantify in each point of the finest grid hazard curves, along with epistemic uncertainty, for two intensity measures: maximum flow depth and maximum momentum flux.

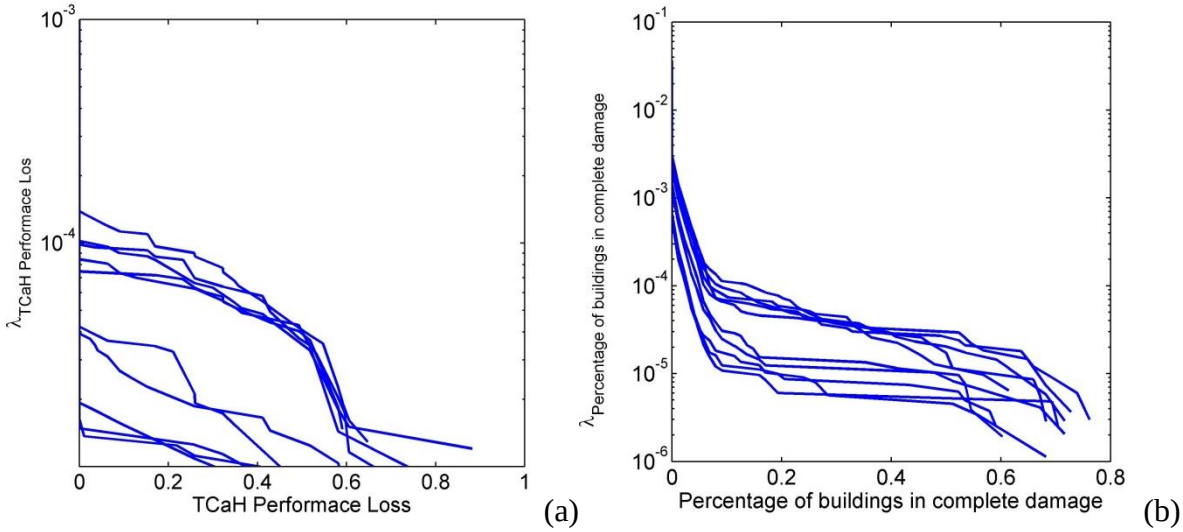

Figure 10. Mean annual frequency (MAF) of exceedance values for the normalized performance loss of the bulk cargo terminal (a) and for the buildings in complete damage state (b) considering alternative models for the tsunami hazard

To assess the tsunami risk a specific hazard module has been developed in order to enable sampling among the 253 representative scenarios, considering the probability of occurrence of the cluster of sources that each scenario represents. This procedure is possible for any preselected alternative model of input to the SPTHA ensemble, enabling the propagation of hazard epistemic uncertainty into risk analysis. The inundation simulation results for each sampled scenario are then loaded, in order to retrieve the tsunami intensity for any selected location. It is noted that, since the SPTHA analysis is based on an explicit simulation of each scenario, spatial correlations of the tsunami intensity are automatically accounted for. Differently from seismic risk, given that inundation does not occur inside buildings (unless they collapse, case not considered in the simulation scheme), tsunami intensity should be retrieved in proximity of each component's perimeter and outside the structure. Therefore, in order to avoid any unwanted biases (e.g., retrieve the tsunami intensity over the roof of buildings, where the modeled tsunami flow depth is subtracted the height of the building), a characteristic radius has been assigned to each component, and the largest intensity value within the defined circle is obtained. Damages and non-functionalities are then sampled from the respective fragility curves (Table 1) and the retrieved tsunami intensities for each individual scenario. The analysis has been implemented for the port infrastructure (cranes, electric power network components and individual buildings) and the PIs for the analyzed system are evaluated. In Fig. 10 we show an indicative example considering ten alternative models of input to the SPTHA ensemble. The differences among the different curves reflect the epistemic uncertainty in the tsunami hazard, showing a considerable dispersion in the loss assessments in terms of TCaH and damaged buildings. The results showed that the container terminal is not expected to experience any loss (TCoH), while the loss in the cargo terminal (TCaH) is negligible. This is due to the non-vulnerable condition of waterfront structures, the high damage thresholds for the cranes (i.e. high inundation values that are not expected in the study area) as described in the fragility curves used in the

application (Fig. 6) and the distance of the electric power substations from the shoreline. The annual probabilities for buildings collapses are also low. As an example 10% of the total buildings in the port (~9 structures) will be completely damaged under tsunami forces with annual probability ranging between 10^{-4} and 10^{-5}. While the port infrastructure seems not much vulnerable to direct damages from tsunami waves, we note that we did not include in our computation the potential effect of collision of debris (e.g., ships). This assumes a good preparedness of the port against tsunamis as well as a rapid and efficient tsunami warning system.

4.2.2 Scenario-based risk assessment

A scenario-based system-wide seismic risk analysis is performed complementary to the classical PRA approach described previously, to quantify the potential impact of the local site response at the port area and to reduce the corresponding uncertainties. As discussed above, this type of effects may be of major importance in port areas, and by adopting specific scenarios is possible to model the site response more accurately than in standard PRA. It is noted that the scenario-based system-wide risk assessment has been carried out only for the seismic hazard as the results of the probabilistic system-wide risk assessment have shown that tsunami hazard is not significant for the application at hand. Two different seismic scenarios were defined: the standard seismic design scenario and an extreme scenario corresponding to return periods of T_m=475 years and T_m=4975 years respectively. To perform the site response analyses a target spectrum for seismic bedrock conditions (shear wave velocity, V_s=700-800 m/s) and a suite of acceleration time histories are needed. For the 475 years scenario, the target spectrum is defined based on the disaggregation of the probabilistic seismic hazard analysis (SRM-LIFE 2007; Papaioannou 2004). This study has shown that the most significant contribution to seismic hazard for Thessaloniki port is associated with the Anthemountas fault system (Papaioannou 2004) situated south of the city of Thessaloniki and practically crossing the gulf (i.e. a normal fault) regardless of the return period. In particular, for the 475 years scenario, the maximum annual exceedance probability for a certain PGA value with a moment magnitude M_w of 5.7 and an epicentral distance R_{epi} of 14.6 km was provided. For the 4975 years scenario, an extreme rupture scenario breaking along the whole Anthemountas fault zone with a magnitude M_w of 7.0, close to the maximum magnitude of the seismic source, was assumed. The GMPE proposed by Akkar and Bommer (2010) is applied, similarly to the probabilistic assessment. In addition to magnitude and distance, both hazard scenarios include an error term ε (which measures the number of standard deviations of logarithmic residuals σ to be accounted for in GMPE) responsible for an appreciable proportion of spectral ordinates. The contribution from ε grows with the return period (Bommer and Acavedo, 2004), thus, the median spectral values plus 0.5 standard deviations and 1 standard deviation are considered for the 475 years and the 4975 years scenarios respectively. This is also in line with the earthquake scenarios selected in Akkar et al. (2014) to generically represent the moderate seismicity (median + 0.5σ for an M_w 6 event) and high seismicity (median + 1σ for an M_w 7 event) regions in Europe. A set of 15 real accelerograms is selected for the 475 years scenario referring to rock or very stiff soils that on average fit the target spectrum. For the extreme scenario, 10 synthetic accelerograms are computed to fit the target spectrum (4975 years scenario I) and

broadband ground motions are generated using 3D physics-based "source-to-site" numerical simulations (4975 years scenario II, Smerzini et al. 2016).

1D equivalent-linear (EQL) and nonlinear (NL) site response analyses including also the potential for liquefaction are carried out for the three soil profiles A, B, and C (see Fig. 3) using as input motions at the seismic bedrock the ones estimated for the 475 years and 4975 years (I and II) seismic scenarios. The numerical codes Strata (Kottke and Rathje 2008) and Cyclic1D (Elgamal et al. 2015) are used for EQL and NL site response analyses respectively. All models assume vertical propagating SH waves from the bedrock to the surface. The liquefaction model employed in Cyclic1D (Parra 1996; Yang 2000) was developed within the framework of multi-yield-surface plasticity (e.g. Prevost 1985). The granular soils (e.g. sands, gravels, non-plastic silts) that are not susceptible to significant pore pressure build-up are simulated using an elastic-plastic material in which a confinement-dependent shear response is considered. For the clay/rock materials, an elastic-plastic material is considered where shear behavior is insensitive to the confinement change.

To investigate the impact of the uncertainty in the shear wave velocity (V_s) profiles, the analyses are performed for the basic geotechnical models, considering a standard deviation of the natural logarithm of the V_s equal to 0.2. In particular, 100 realizations of the V_s profiles are considered in Strata using Monte Carlo simulations and the calculated response from each realization is then used to estimate statistical properties of the seismic response. In total 1500 and 1200 simulations are performed for the 475 and 4975 (I and II) scenarios respectively. The randomization of the V_s and the incorporation in Monte Carlo simulations are performed through the model proposed by Toro (1995). The corresponding site response variability was assessed in Cyclic1D considering except for the basic V_s model, upper-range and lower-range models utilizing a logarithmic standard deviation for the V_s profile equal to 0.2 consistently with the Strata simulations. For the EQL approach the results are presented in terms of PGA variation with depth, acceleration response spectra and spectral and Fourier ratios. For the NL approach, the variation of horizontal and vertical PGD, maximum shear strain and stress, effective confinement and excess pore water pressure with depth were also computed for each analysis. Comparative plots between the EQL and NL approaches are shown in Fig. 11 for the 475 years and 4975 years I scenarios for profile A while Fig. 12 depicts indicative results of the NL analysis for the selected input motions for the same soil profile.

The spectral values and shapes are generally well compared between the two approaches for the 475 years scenario while the response is very different for the extreme scenario that is associated with increasing shear strain accumulation. For both scenarios, the EQL spectral shapes are flatter and have less period-to-period fluctuations than the NL ones. The lower spectral values predicted by the NL approach for the extreme seismic scenario could be attributed to the liquefaction, which cannot be simulated by the EQL analysis. The results of the NL approach indicate that liquefaction is evident for all soil profiles and scenarios. However, for the extreme scenario, the liquefiable layers are larger and extended to greater depths (up to 35m, e.g. see Fig. 12a,b). Among the three representative soil profiles, liquefaction effects are shown to be more pronounced in profile A. Large variability in the computed permanent displacements is shown for the different seismic input motions (e.g. see Fig. 12c,d). Generally, low-frequency input motions increase the accumulation of lateral deformations and settlements. The computed maximum horizontal displacement

values when considering the basic geotechnical models are 4.5 cm and 18.6 cm for the 475 and 4975 years seismic scenarios respectively, while the corresponding values for the vertical displacements (settlements) are 4.8 cm and 11.0 cm.

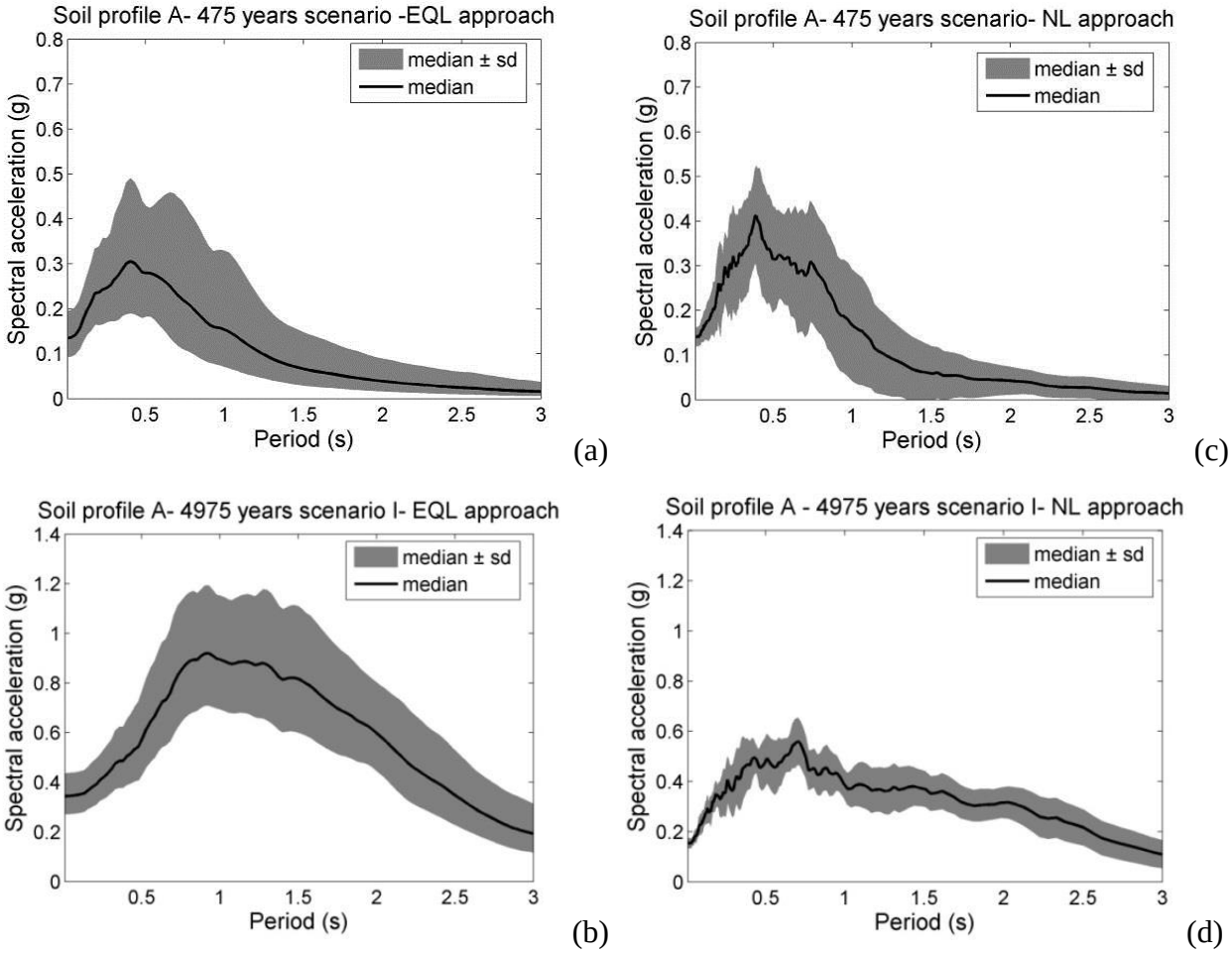

Figure 11. Median ± standard deviation elastic 5% response spectra at the ground surface for soil profile A using the EQL (a, b) and NL (c, d) approaches for the 475 years scenario and the 4975 years scenario

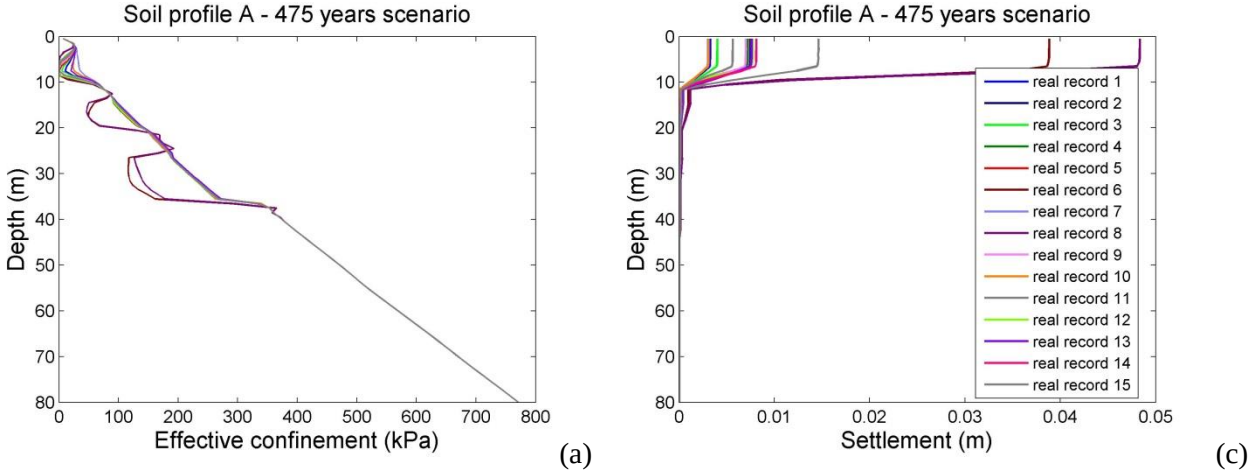

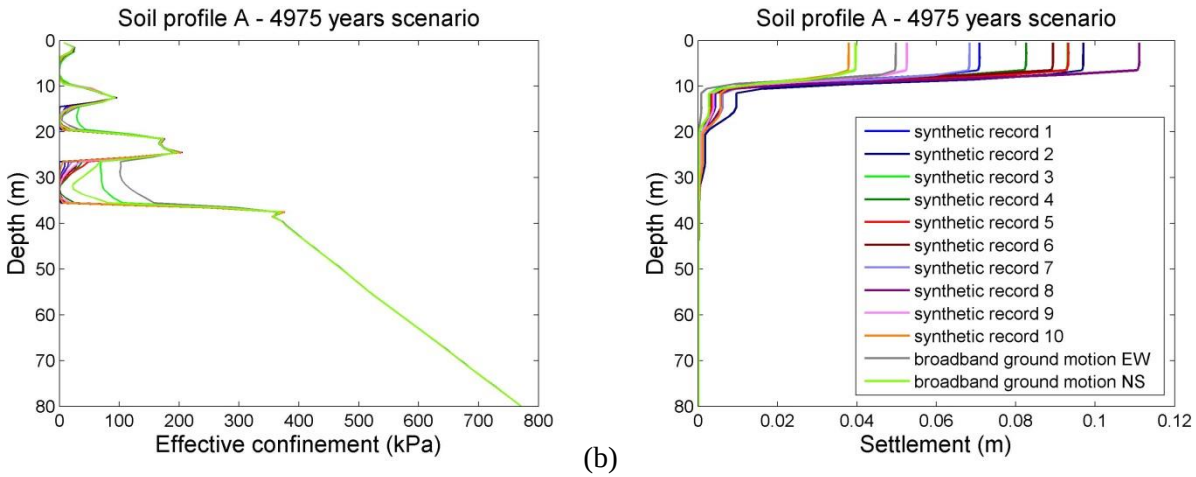

(b)

(d)

Figure 12. Variation of effective confinement (a, b) and settlement with depth (c, d) for soil profile A for the 475 years scenario and the 4975 years scenario

The scenario-based risk assessment of the port buildings and infrastructures is initially performed taking into account the potential physical damages and corresponding losses of the different components of the port. Buildings, waterfront structures, cargo handling equipment and the power supply system are examined using the fragility models for ground shaking and liquefaction (Table 1). In particular, the vulnerability assessment is performed for the 475 and 4975 years scenarios (I and II) based on the EQL and NL site-response analyses. The results from response analyses of soil profiles A, B or C were considered in the fragility analysis, depending on the proximity of each component to the location of the three soil profiles. In particular, for the EQL approach, the calculated PGA values at the ground surface from the total analysis cases (i.e. 2200 analyses) for each soil profile were taken into account for the vulnerability assessment due to ground shaking. For the NL approach, except for the PGA values, the PGD (horizontal and vertical) values at the ground surface were also considered to evaluate the potential damages to buildings and infrastructures due to liquefaction effects. Finally, the combined damages are estimated by combining the damage state probabilities due to the liquefaction (P_L) and ground shaking (P_{GS}), based on the assumption that damage due to ground shaking is independent and not affect the damage due to liquefaction (NIBS, 2004). Once the probabilities of exceeding the specified DS are estimated, a median ±1 standard deviation damage index d_m is evaluated, to quantify the structural losses as the ratio of cost of repair to cost of replacement taking values from 0: no damage (cost of repair equals 0) to 1: complete damage (cost of repair equals the cost of replacement). In case of buildings, a weighted loss index (WLI) is calculated to weight the damage index with respect to the built area.

The spatial distribution of the estimated losses for buildings indicates that a non-negligible percentage of the port buildings are expected to suffer significant losses (higher than moderate). The median values of this percentage range from 7% for the design scenario (NL approach) to 37% for the 4975 years scenario I (EQL approach) (e.g. see Figure 13). This is expectable taking into account that all buildings were constructed with

low or no seismic code provisions. Among the considered building typologies, the RC structures appear to be less vulnerable compared to the steel and URM systems.

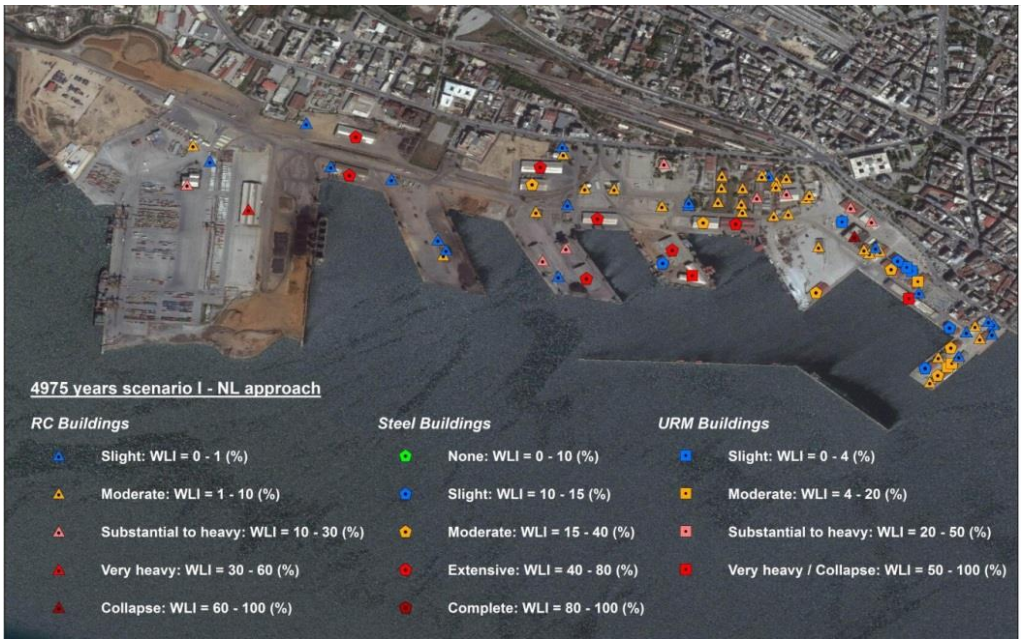

Figure 13. 4975 years scenario I- NL approach: spatial distribution of the losses of Thessaloniki's port buildings

The estimated losses are also significantly dependent on the analysis approach. In particular, the EQL approach is associated with higher damages and losses even for the design scenario, while for the NL approach the losses to the cranes, waterfronts, and electric power substations are expected solely for the 4975 scenario I. The larger damages and losses computed by the EQL approach for port buildings and infrastructures could be attributed to the significantly higher PGA values calculated using the EQL approximation, which lead to higher damage probabilities. Thus, even though the vulnerability using the NL approach is assessed considering both ground shaking and liquefaction hazards, the estimated combined exceedance probabilities are still lower compared to the ones predicted by the EQL approach.

The systemic risk consequent to the selected scenarios is assessed following the methodology presented in the previous section (PRA approach) that accounts the interdependencies of specific components. It is observed that the EQL approach is associated with higher number of non-functional components for all considered seismic scenarios whereas for the NL approach non-functional components are present only for the 4975 years scenario I. The estimated PIs of the port are normalized to the respective value referring to non-seismic conditions. Table 4 presents the PIs of the port system in terms of the median normalized performance loss ($1\text{-}PI/PI_{max}$) for the different analysis approaches and seismic scenarios. As also evidenced by the estimated functionality state of each component, the port system is non-functional both in terms of TCaH and TCoH for the 4975 years scenario I. A 100% and 67% performance loss is estimated for the TCoH and TCaH respectively when considering the EQL approach for the 475 years and 4975 years II scenarios, while the port is fully functional when considering the NL approach both in terms of TCaH and TCoH for the latter scenarios. It is noted that the estimated PIs do not change when considering the

median+1standard deviation damage indices in the computation of the components' functionality. However, when the median-1standard deviation damage indices are taken into account in the calculations, a 100% performance loss is estimated only for the 4975 years scenario I while the port is fully functional for all the other analysis cases both in terms of TCaH and TCoH.

Table 4. Estimated median normalized performance loss of the port system for TCaH and TCoH and comparison with risk objectives for the scenario-based assessment

Scenario	Analysis type	Performance loss ($1-PI/PI_{max}$)		Risk objectives			Stress test outcome	
		TCaH	TCoH	AA-A	A-B	B-C	TCaH	TCoH
475 years	EQL	0.67	1.00	0.10	0.30	0.50	Fail	Fail
	NL	0.00	0.00				Pass	Pass
4975 years I	EQL	1.00	1.00	0.30	0.50	0.70	Fail	Fail
	NL	1.00	1.00				Fail	Fail
4975 years II	EQL	0.67	1.00				Partly pass	Fail
	NL	0.00	0.00				Pass	Pass

5. DECISION PHASE

The Decision phase comprises different steps including (i) the comparison of the assessment results with the pre-defined risk objectives, (ii) disaggregation and/or sensitivity analysis to identify critical events and components and (iii) formulation of guidelines and risk mitigation strategies to improve the performance of the port.

5.1 Risk objectives check

In the first step of the decision phase, the risk assessment results are compared with the defined risk objectives to check whether the port system passes, partially passes or fails the stress test and to define the grading system parameters for the next evaluation of the stress test since the performance of the CI or performance objectives can change over time.

In Fig. 14 risk boundaries are plotted together with the MAF curves of the assessed performance loss. With reference to seismic hazard for both bulk cargo and container terminals (TCaH, TCoH curves in Fig 14a) the port obtains grade B, meaning that the risk is possibly unjustifiable and the CI partly passes this evaluation. The basis for the redefinition of risk objectives in the next evaluation of stress test is the characteristic point of risk, which is defined as the point associated with the greatest risk above the ALARP region (blue and red dots for TCaH and TCoH curves respectively). These points are the farthest from the A-B boundary (blue line). The proposed grading system foresees the reduction of the boundary between grades B and C (red line) in the next stress test, which is equal to the amount of risk beyond the ALARP region assessed, represented in this application by the corresponding red dashed lines in case of the bulk cargo and cargo terminals. The plot in Fig. 14b indicates that the CI receives grade AA (negligible risk) in case of the tsunami hazard, and as expected in this example application for one of the representative scenarios the CI passes the stress test.

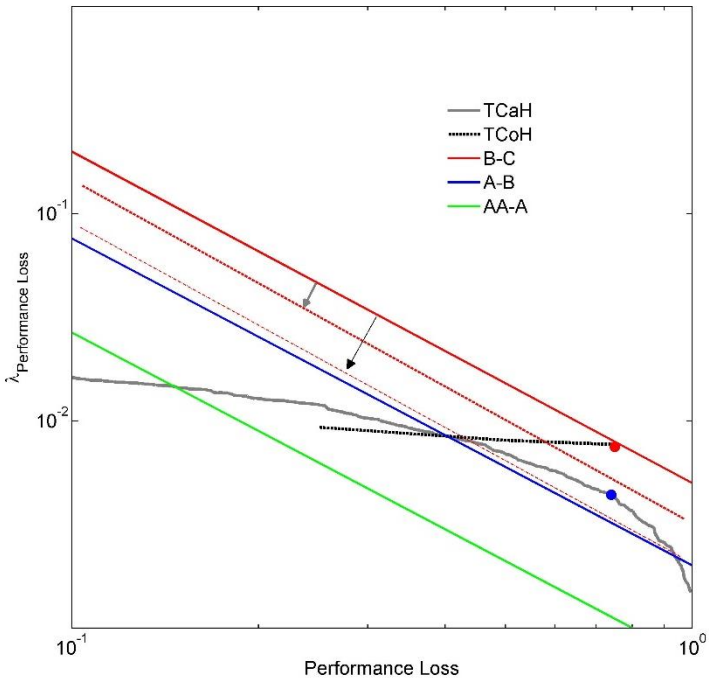

(a)

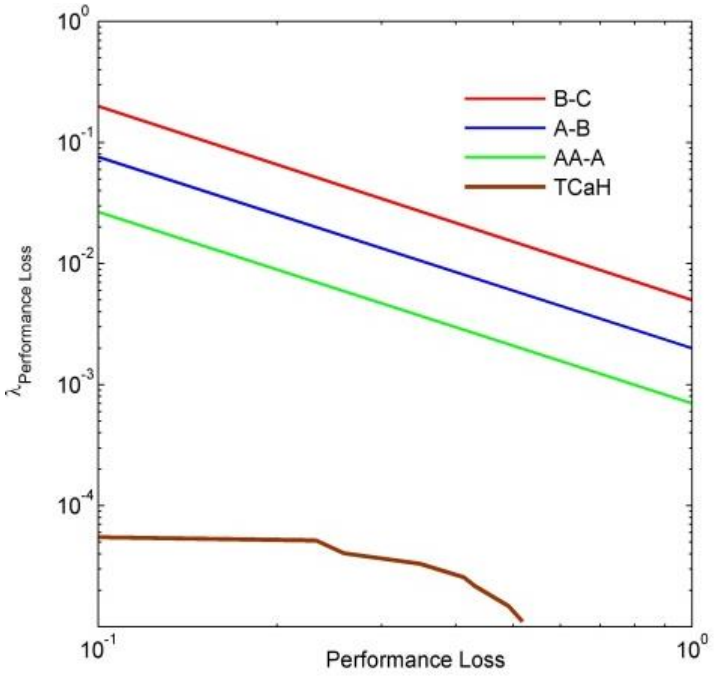

(b)

Figure 14. Mean annual frequency (MAF) of exceedance values for the normalized performance loss of the bulk cargo (TCaH) and container (TcoH) terminal for the ground shaking (a) and the tsunami (b) hazard case. The green, blue and red continuous lines correspond to the boundaries between risk grades AA (negligible), A (ALARP), B (possibly unjustifiable risk), and C (intolerable)

Indicative scalar performance boundaries in terms of the normalized performance loss are shown in Table 4 together with the corresponding results of the scenario-based assessment. It is seen that the CI may pass, partly pass or fail for the specific evaluation of the stress test (receiving grades AA, B and C respectively) depending on the selected seismic scenario, the analysis approach and the considered risk metric (i.e. TCaH, TCoH). These results show that the impact of high-quality modeling of local site effects is of major importance and that accounting for this in PRA would probably lead to lower grading. Nevertheless, it is pointed out that the grading for the scenario-based approach is complementary; in practice the risk objectives check and the definition of next stress test are based in the PRA results. It is also worth noting that the risk objectives and the time between successive stress tests should be defined by the CI authority and regulator. Since regulatory requirements do not yet exist for the port infrastructures, the boundaries need to rely on judgments.

5.2 Disaggregation Analysis

In order to evaluate the contribution of certain components on the overall performance of the network, the correlation between damaged components and system's functionality is estimated. For Stress Test Levels 2 (System Level Assessment for Single Hazard ST-L2), the most critical elements for the functionality of the port system are defined through correlation factors to the system PIs based on all simulations. This type of analysis, as it is based on the results of every single event, preserves the information about system's topology, its behavior in case of spatially correlated damages (related to single events) and functional inter-dependencies (e.g., Argyroudis et al. 2015). Thus, it allows identifying the most critical elements for the functionality of the port system (i.e., the damaged components that tend to control the performance of the harbor). For the case of PRA for ground shaking Figures 15 and 16 show the level of correlation (low,

medium, high) between the TCaH and TCoH and the distribution of damages in cranes and the non-functionality of electric power distribution substations respectively. In this way, the most critical components can be identified in relation to their contribution to the performance loss of the system.

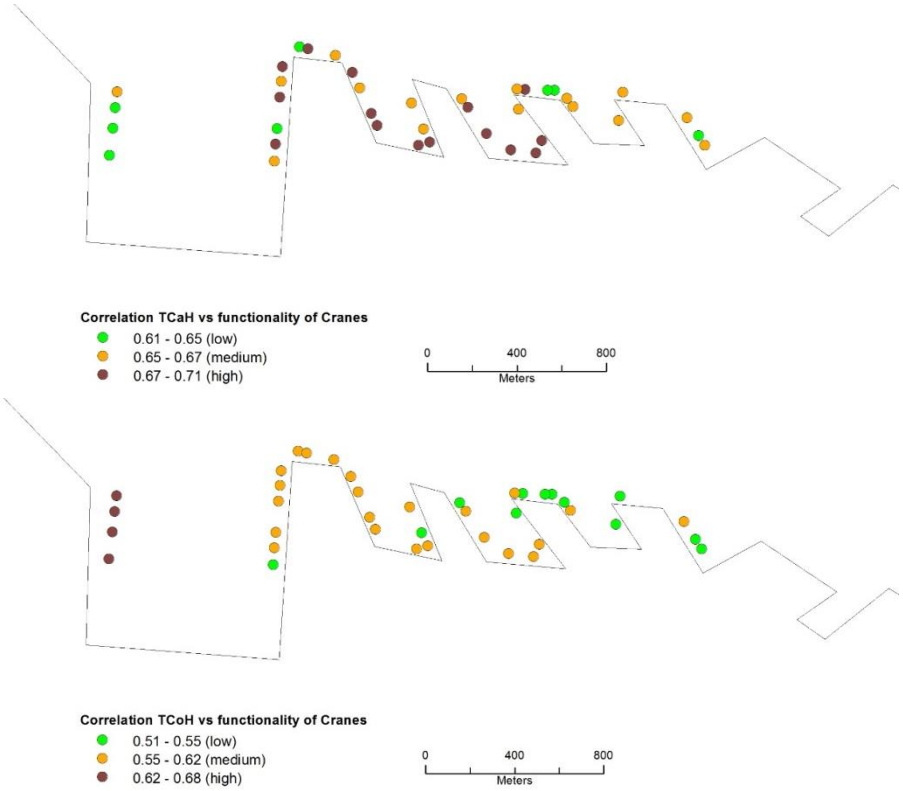

Figure 15. Correlation of damaged cranes to port performance (TCaH and TCoH) for ST-L2 due to ground shaking

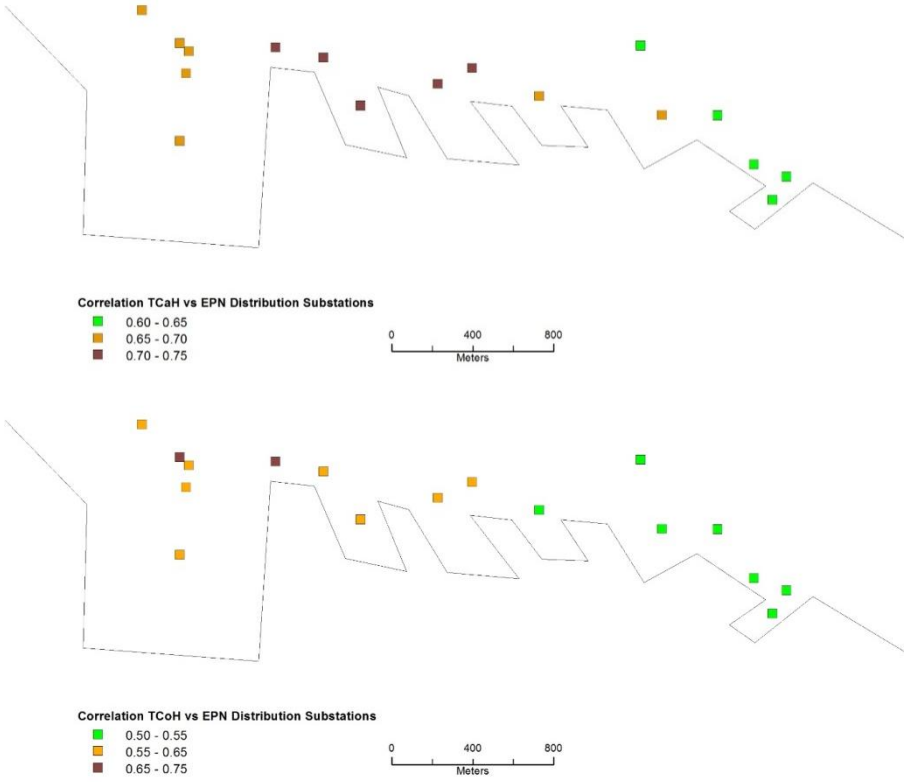

Figure 16. Correlation of non-functional EPN distribution substations to port performance (TCaH and TCoH) for ST-L2 due to ground shaking

5.3 Guidelines

For the selected target probabilities of collapse, all port components are deemed as unsafe towards seismic hazards at the component level assessment, while only a few cranes are characterized as safe against exceedance of the collapse limit state for the tsunami hazard. These results cannot be judged unconditional to the fact that regulatory requirements for port infrastructures do not yet exist and the boundaries rely on judgments.

For ST-L2, and for the seismic case, several electric power distribution substations present high failure risk and contribute to the performance loss of the port due to loss of power supply to the cranes. It is recommended to investigate further the response of the substations under seismic shaking and consider the potential upgrade or/and alternative power sources such as diesel generators. The systemic risk for the tsunami hazard is very low, however, it is recommended to extend the model and investigate the effect of floating ships that may hit the different components of the harbor, which is now neglected.

For the scenario-based assessment, the estimated losses are significantly dependent on the analysis approach. In particular, the EQL approach is associated with higher losses even for the design scenario (475 years), while for the NL approach the losses to the cranes, waterfronts, and electric power substations are expected solely for the 4975 scenario I. Among the four different outcomes determined for the extreme scenario for both PIs, the CI passes the stress test in the 4975 years scenario II and NL method, which could be judged as the most reliable.

The tsunami risk connected to direct damages from waves results is not significant. This is primarily connected to the physical position of the port (with relatively low tsunami hazard) and the low fragility of components to tsunami waves. However, the potential effect of debris collisions has not been accounted for. Therefore, a careful check of preparedness against tsunamis should be suggested, ranging from the connection to efficient tsunami warning systems as well as the definition of actions to secure ships and port equipment in case of a tsunami.

In general, the risk mitigation strategies include preventive (i.e. before the occurrence of a disaster) and reactive (i.e. after the disaster) measures, designed to reduce the likelihood and severity of the various types of port disruptions (Lam and Su 2015). The preventive measures include early warning systems for earthquakes and tsunami (Cauzzi et al. 2015; Wachter et al 2012), retrofitting of vulnerable buildings, improvement of foundation soil or quay wall backfills (Tsinker 2004, Dakoulas and Gazetas 2005), strategic alliances with nearby ports for crisis periods, updating of contingency plans and training exercises. The reactive measures are related to the rapidity of restoration, which depends on the availability of resources and recovery crews and the efficiency of emergency planning. The latter should take into account the importance of the port components, the recovery priorities and the buffering capabilities, which allow a given asset to temporarily provide service under perturbed operational conditions (e.g. use of mobile cranes or diesel generators during the recovery operations to substitute any damaged cranes or electric power substations respectively). These factors have been recently taken into account by Galbusera et al (2018) to simulate the recovery process of selected infrastructures of the Thessaloniki Port in a given earthquake scenario based on a dynamic Boolean network approach.

6. CONCLUSIONS

The recently developed methodology for stress test of critical non-nuclear infrastructures was applied to the port infrastructure of Thessaloniki, Greece exposed to different seismic hazards, i.e. ground shaking, liquefaction and tsunami. The vulnerability assessment of the infrastructures to the given hazards was performed using site and case-specific or generic fragility functions. Specific risk metrics and objectives were defined related to the functionality of the port system and the structural losses. In the first level of the assessment phase, a risk-based assessment of each component was carried out for earthquake and tsunami hazards to check its performance. To accomplish that, the target (acceptable) probability of collapse implied by the code, stakeholders and decision-makers needs was pre-defined for each component. Then, a probabilistic risk analysis was conducted for the whole system separately for earthquake and tsunami hazards considering specific interdependencies between network and components. Site-specific response and extreme seismic events were evaluated with a scenario-based system-wide risk analysis. In the decision phase, the estimated response was compared with predefined risk objectives in order to assess the performance of the port and decide whether it passes, partly passes or fails the test for all possible events and to define how much the safety of the port should be improved until the next periodical verification. Since no regulatory boundaries exist for port facilities, the risk objectives in this application were defined as continuous and scalar boundaries based on general judgment criteria for the probabilistic and scenario-based system-wide

risk assessment respectively. It has been shown that the port obtains grades B (the risk is possibly unjustifiable) and AA (negligible risk) for the PRA of earthquake and tsunami hazards respectively, meaning that the port partly passes or passes this evaluation of the stress test. The comparison of the scenario-based assessment response with the risk objectives indicates that the port may pass, partly pass or fail for the specific evaluation of the stress test depending on the selected seismic scenario, the analysis approach, and the considered risk metric. However, since the scenario-based approach is complementary to the PRA, this grading is indicative and the grading results from the PRA provide the basis for the decision phase and the definition of next stress test. A next step of the decision phase is the identification of the critical components and events as well as the recommendation of risk mitigation strategies to upgrade the port operations and improve its resilience. Finally, in the Report phase, the outcome of the stress test (in terms of grades, critical events/components, guidelines for risk mitigation) is communicated to the Port Authority. Based on the different outcomes of the stress test, it is up to the Port Authority to decide to take specific measures to improve and upgrade or not the performance and thus the reliability of the port.

The methodology can be adapted and applied to other port infrastructure including additional components, interdependencies, and hazards as well as performance indicators. In this context, future studies may consider the vulnerability of the electric power lines and electric poles due to earthquake and tsunami hazards using recently available fragility curves (e.g. by Kongar et al 2017 for buried cables subject to ground shaking and liquefaction). Also, future work may include modeling of other interdependencies such as water and oil/gas supply to critical buildings and vessels, as well interconnections with the railway and highway networks, which play a key role for the port operations in unperturbed conditions and in the recovery following a disaster.

ACKNOWLEDGMENTS

The work reported in this paper was carried out in the framework of STREST project, funded by the European Community's Seventh Framework Programme (FP7/2007-2013) under grant agreement no. 603389. The contribution of Volpe M, Tonini R, Romano F, Brizuela B, Piatanesi A, Basili R, Lorito S. (INGV, Italy) in the tsunami hazard analysis is acknowledged. The support of Thessaloniki Port Authority S.A is also acknowledged, in particular, we would like to thank Mr. Emmanouil Michailidis, General Director of Operational Units, and Dr Savvas Sismanis, Estate-Works Development Director.

REFERENCES

Aki K. Space and Time Spectra of Stationary Stochastic Waves, with Special Reference to Microtremors. Bull Earthq Res Inst Tokyo Univ 1957; 25:415-457.

Akkar S, Bommer JJ. Empirical equations for the prediction of PGA, PGV and spectral accelerations in Europe, the Mediterranean and the Middle East. Seismol Res Lett 2010; 81: 195–206.

Alises A, Molina R, Gómez R, Pery P, Castillo C. Overtopping hazards to port activities: Application of a new methodology to risk management (POrt Risk MAnagement Tool), Reliab Eng Syst Saf 2014; 123:8-20.

Anastasiadis A, Raptakis D, Pitilakis K. Thessaloniki's detailed microzoning: subsurface structure as basis for site response analysis, Pure Appl Geophys 2001; 158:2597-2633.

803 Apostolidis P, Raptakis D, Roumelioti Z, Pitilakis K. Determination of S-wave velocity structure using microtremors
804 and spac method applied in Thessaloniki (Greece). Soil Dyn Earthq Eng 2004; 24:49-67.
805 Argyroudis S, Selva J, Gehl P, Pitilakis K, Systemic seismic risk assessment of road networks considering interactions
806 with the built environment, Computer-Aided Civil and Infrastructure Engineering 2015; 30 (7): 524-540.
807 Basili R, Tiberti MM, Kastelic V, Piatanesi A, Selva J, Lorito S. Integrating geologic fault data into tsunami hazard
808 studies. Nat Hazards Earth Syst Sci 2013; 13:1025-1050, DOI: 10.5194/nhess-13-1025-2013.
809 Berle O, Asbjørnslett BE, Rice JB. Formal vulnerability assessment of a maritime transportation system. Reliab Eng
810 Syst Saf 2011; 115:136-45.
811 Bommer JJ, Acevedo AB. The use of real accelerograms as input to dynamic analysis. J Earthq Eng 2004; 8(1):43-91;
812 DOI: 10.1080/13632460409350521.
813 Calvi GM, Pinho R, Magenes G, Bommer JJ, Restrepo-Velez LF, Crowley H. 2006. The development of seismic
814 vulnerability assessment methodologies for variable geographical scales over the past 30 years. ISET Journal of
815 Earthquake Technology 2006; 43(3).
816 Cauzzi C, Sousa Oliveira C, Emolo A, Zollo A, Zülfikar C, Pitilakis K, Vogfjord K, Lai C, Sokos E, Erdik M, Şafak E,
817 Gasparini P, Wiemer S, Zschau J, Behr Y, Clinton J, Esposito S, Colombelli S, Picozzi M, Karapetrou S, Bindi D,
818 Zuccolo E, Parolai S, Miranda N, Ferreira M, Jonsdottir K. Towards Real-time Risk Reduction for Strategic
819 Facilities through Earthquake Early Warning: summary of the REAKT experience. Seismological Research Letters
820 2015; 86(2B):696-696, DOI.10.1785/0220150017.
821 Chang SE (2000). Transportation performance, disaster vulnerability, and long-term effects of earthquakes. In:
822 Proceedings of the 2nd EuroConference on Global Change and Catastrophe Risk Management, Laxenburg, Austria.
823 Cornell C, Krawinkler H. Progress and challenges in seismic performance assessment. PEER News 2000; 3(2).
824 Cotton F et al. 2015, Deliverable 3.7: Multi-hazard assessment of low-probability hazard and LP-HC events for six
825 application areas, STREST project: Harmonized approach to stress tests for critical infrastructures against natural
826 hazards; 2015.
827 Crowley H, Casotto C, Pitilakis K, Kakderi K, Argyroudis S, Fotopoulou S, Lanzano G, Salzano E, Iervolino I, Basco
828 A, Matos JP, Schleiss A, Uckan E, Miraglia S, Courage W. Deliverable D4.4: Report on the taxonomy of CIs based
829 on their vulnerability characteristics and exposure to natural hazard initiating events. STREST project: Harmonized
830 approach to stress tests for critical infrastructures against natural hazards; 2016.
831 Dakoulas P, Gazetas G. Seismic effective-stress analysis of caisson quay walls: Application to Kobe. Soils and
832 Foundations 2005; 45(4):133-147.
833 Davies G, Griffin J, Lovholt F, Glimsdal S, Harbitz C, Thio HK, Lorito S, Basili R, Selva J, Geist E, Baptista MA. A
834 global probabilistic tsunami hazard assessment from earthquake sources, in Tsunamis: Geology, Hazards and Risks
835 (Scourse EM, Chapman NA, Tappin DR & Wallis SR Eds), Geological Society, London, Special Publications,
836 2018; SP456, https://doi.org/10.1144/SP456.5
837 Elgamal A, Yang Z, Lu J. Cyclic1D Seismic Ground Response Version 1.4. User's Manual, University of California,
838 San Diego; Department of Structural Engineering; 2015.
839 EN 1998-1. Eurocode 8: Design of structures for earthquake resistance-Part 1: General rules, seismic actions and rules
840 for buildings. CEN, Bruxelles; 2004.
841 Erdik 2000. Report on 1999 Kocaeli and Duzce (Turkey) Earthquakes. In: Proceedings of the 3rd International
842 Workshop on Structural Control. Paris-France, 6-8 July 2000; pp. 149-186.

Esposito S, Stojadinović B, Babič A, Dolšek M, Iqbal S, Selva J. Engineering risk-based methodology and grading system for stress testing of critical non-nuclear infrastructures (STREST Project). In: Proceedings of the 16th World Conference on Earthquake Engineering. Santiago, Chile; 9-13 January 2017.

Eusgeld I, Nan C, Dietz S. "System-of-systems" approach for interdependent critical infrastructures. Reliab Eng Syst Saf 2011; 96(6):679-686.

Fajfar P, Dolšek M. A practice-oriented estimation of the failure probability of building structures. Earthq Eng Struct Dyn 2012; 41(3):531–547.

Filippini R, Silva A. A modeling framework for the resilience analysis of networked systems-of-systems based on functional dependencies. Reliab Eng Syst Saf 2014; 125:82-91.

Fotopoulou S, Pitilakis K. Fragility curves for reinforced concrete buildings to seismically triggered slow-moving slides, Soil Dyn Earthq Eng 2013; 48:143–161.

Galbusera L, Giannopoulos G, Argyroudis S, Kakeri K. A Boolean Networks approach to modeling and resilience analysis of interdependent critical infrastructures. Computer-Aided Civil and Infrastructure Engineering 2018; (in press).

Giardini D. et al. Seismic Hazard Harmonization in Europe (SHARE). Online Data Resource, http://portal.share-eu.org:8080/jetspeed/portal/; doi: 10.12686/SED-00000001-SHARE; 2013.

Gonzalez Vida JM et al. Tsunami-HySEA: a GPU based model for the Italian candidate tsunami service provider. EGU General Assembly; Vienna, Austria; 12-17 April 2015; Abstract # EGU2015-13797.

Grezio A, Babeyko A, Baptista MA, Behrens J, Costa A, Davies G, Geist E, Glimsdal S, Gonzales FI, Griffin J, Harbitz C, LeVeque RJ, Lorito S, Lovholt F, Omira R, Mueller C, Paris R, Parsons T, Polet J, Power W, Selva J , Sorensen MB, Thio HK, Probabilistic Tsunami Hazard Analysis: Multiple Sources and Global Applications. Reviews of Geophysics 2017; 55, DOI:10.1002/2017RG000579.

Groen FJ, Smidts C, Mosleh A. QRAS-the quantitative risk assessment system. Reliab Eng Syst Saf 2006; 91(3):292-304.

Guedes Soares C, Teixeira AP. Risk assessment in maritime transport. Reliab Eng Syst Saf 2001; 74:299-309.

Hsieh C-H, Tai H-H, Lee Y-N. Port vulnerability assessment from the perspective of critical infrastructure interdependency. Maritime Policy & Management 2014; 41(6):589-606.

Ichii K. Fragility curves for gravity-type quay walls based on effective stress analyses. In: Proceedings of the 13th World Conference on Earthquake Engineering. Vancouver, BC Canada; 2004.

Jayaram N, Baker JW. Correlation model of spatially distributed ground motion intensities. Earthq Eng Struct Dyn 2009; 38(15):1687–1708.

Kakderi K, Fotopoulou S, Argyroudis S, Karafagka S, Pitilakis K, Anastasiadis A, Smerzini C, Selva J, Giannopoulos G, Galbusera L, Courage W, Reinders J, Cheng Y, Akkar S, Erdik M, Uckan E. 2015. Deliverable D4.2: Guidelines for performance and consequences assessment of geographically distributed, non-nuclear critical infrastructures exposed to multiple natural hazards. STREST project: Harmonized approach to stress tests for critical infrastructures against natural hazards; 2015.

Kakderi K, Pitilakis K. Seismic performance and reliability of port facilities – The case of Thessaloniki (Greece). In: Proceedings of the 5th International Conference on Recent Advances in Geotechnical Earthquake Engineering and Soil Dynamics and Symposium in Honor of Professor I.M. Idriss. San Diego, California; 2010; Paper 6.04a.

Kappos AJ, Panagiotopoulos C, Panagopoulos G, Panagopoulos El. WP4-Reinforced concrete buildings (Level I and II analysis). RISK-UE: An advanced approach to earthquake risk scenarios with applications to different European towns; 2003.

885 Kappos AJ, Panagopoulos G, Panagiotopoulos C, Penelis G. A hybrid method for the vulnerability assessment of R/C
886 and URM buildings. B Earthq Eng 2006; 4:391-419.
887 Karafagka S, Fotopoulou S, Pitilakis K. Tsunami fragility curves for seaport structures. In: Proceedings of the 1st
888 International Conference on Natural Hazards & Infrastructure. Chania, Greece; 28-30 June 2016.
889 Kongar I, Giovinazzi S, Rossetto T. Seismic performance of buried electrical cables: evidence-based repair rates and
890 fragility functions. B Earthq Eng 2017; 15(7):3151-3181.
891 Kosbab BD. Seismic performance evaluation of port container cranes allowed to uplift. PhD thesis; School of Civil and
892 Environmental Engineering, Georgia Institute of Technology; 2010.
893 Kottke AR, Rathje EM. Technical Manual for Strata. University of California, Berkeley; PEER Report 2008/10.
894 Kourkoulis R, Gelagoti F, Loli M, Gazetas G. Interplay of container port cranes and Quay-Walls during earthquake
895 shaking. In: Proceedings of the 2nd European Conference on Earthquake Engineering and Seismology. Istanbul; 25-
896 29 Aug 2014.
897 Lam JSL, Lassa JA. Risk assessment framework for exposure of cargo and ports to natural hazards and climate
898 extremes. Maritime Policy & Management 2017; 44(1):1-15.
899 Lam JSL, Su S. Disruption risks and mitigation strategies: an analysis of Asian ports. Maritime Policy & Management
900 2015; 42(5):415-435.
901 Lazar N, Dolšek M. Application of the risk-based seismic design procedure to a reinforced concrete frame building. In:
902 Proceedings of the 4th ECCOMAS Thematic Conference on Computational Methods in Structural Dynamics and
903 Earthquake Engineering. M. Papadrakakis, V. Papadopoulos, V. Plevris (eds.) Kos Island, Greece; 12–14 June 2013.
904 Lorito S, Selva J, Basili R, Romano F, Tiberti MM. Piatanesi A. Probabilistic hazard for seismically-induced tsunamis:
905 accuracy and feasibility of inundation maps, Geophys J Int 2015; 200(1):574-588.
906 Marzocchi W, Taroni M, Selva J. Accounting for epistemic uncertainty in PSHA: logic tree and ensemble modeling,
907 Bull Seismol Soc Am 2015; 105(4); doi: 10.1785/0120140131.
908 Miraei M, Jafarian Y. Fragility curves for assessing the seismic vulnerability of gravity quay walls. In: Proceedings of
909 the COMPDYN in 4th ECCOMAS Thematic Conference on Computational Methods in Structural Dynamics and
910 Earthquake Engineering Papadrakakis M, Papadopoulos V, Plevris V (eds). Kos Island, Greece; 2013.
911 Molinari I, Tonini R, Lorito S, Piatanesi A, Romano F, Melini D, Hoechner A, Gonzàlez Vida JM, Maciás J, Castro MJ,
912 de la Asunción M. Fast evaluation of tsunami scenarios: uncertainty assessment for a Mediterranean Sea database.
913 Nat Hazards Earth Syst Sci 2016; 16(12):2593.
914 Na UJ, Shinozuka M. (2009). Simulation-based seismic loss estimation of seaport transportation system. Reliab Eng
915 Syst Saf 2009; 94(3):722-731.
916 Nan C, Sansavini G. A quantitative method for assessing resilience of interdependent infrastructures. Reliab Eng Syst
917 Saf 2017; 157:35-53.
918 National Institute of Building Sciences, NIBS. Direct physical damage-general building stock. HAZUS-MH Technical
919 manual, Chapter 5. Federal Emergency Management Agency. Washington, D.C; 2004.
920 NCEER. The Hanshin-Awaji Earthquake of January 17, 1995: Performance of Lifelines, Technical Report NCEER-95-
921 0015 (Ed. M. Shinozuka). State University of New York, Buffalo; 1995.
922 Ouyang M. Review on modeling and simulation of interdependent critical infrastructure systems. Reliab Eng Syst Saf
923 2014; 121:43-60.
924 Pachakis D, Kiremidjian AS. Estimation of downtime-related revenue losses in seaports following scenario
925 earthquakes, Earthq Spectra 2004; 20(2):427-449.

926 Papaioannou C. Seismic hazard scenarios-Probabilistic seismic hazard analysis, SRM-Life Project: Development of a
927 global methodology for the vulnerability assessment and risk management of lifelines, infrastructures and critical
928 facilities. Application to the metropolitan area of Thessaloniki (in greek), 2004.
929 Parra E. Numerical Modeling of Liquefaction and lateral Ground Deformation including Cyclic Mobility and Dilative
930 Behavior is Soil Systems. PhD Dissertation; Department of Civil Engineering; Rensselaer Polytechnic Institute, Try,
931 NY; 1996.
932 PIANC. Seismic Design Guidelines for Port Structures. International Navigation Association, Balkema, 2001, p. 474.
933 Pitilakis K, Anastasiadis A. Soil and site characterization for seismic response analysis. In: Proceedings of the XI
934 ECEE. Inv Lectures, Paris, 6-11 Sept 1998, pp.65-90.
935 Pitilakis K, Argyroudis S, Fotopoulou S, Karafagka S, Anastasiadis A, Pitilakis D, Raptakis D, Riga E, Tsinaris A,
936 Mara K, Selva J, Iqbal S, Volpe M, Tonini R, Romano F, Brizuela B, Piatanesi A, Basili R, Salzano E, Basco A,
937 Schleiss AJ, Matos JP, Akkar S, Cheng Y, Uckan E, Erdik M, Courage W, Reinders J, Crowley H, Rodrigues D.
938 Deliverable D6.1: Integrated report detailing analyses, results and proposed hierarchical set of stress tests for the six
939 CIs. EU FP7 research project No 603389: STREST; 2016.
940 Pitilakis K, Crowley H., Kaynia A (Eds). SYNER-G: Typology definition and fragility functions for physical elements
941 at seismic risk. Buildings, lifelines, transportation networks and critical facilities. Geotechnical, Geological and
942 Earthquake Engineering. Netherlands, 27, Springer, 2014a.
943 Pitilakis K, Franchin P, Khazai B, Wenzel H. (Eds). SYNER-G: Systemic seismic vulnerability and risk assessment of
944 complex urban, utility, lifeline systems and critical facilities. Methodology and applications. Geotechnical,
945 Geological and Earthquake Engineering. Netherlands, 31, Springer, 2014b.
946 Prevost JH. A Simple Plasticity Theory for Frictional Cohesionless Soils. Soil Dyn Earthq Eng 1985; 4(1): 9-17.
947 Rinaldi SM, Peerenboom JP, Kelly TK. Identifying, understanding, and analyzing critical infrastructure
948 interdependencies. IEEE Control Systems Magazine 2001; 21(6):11–25.
949 Salzano E, Basco A, Karafagka S, Fotopoulou S, Pitilakis K, Anastasiadis A, Matos JP, Schleiss AJ. Deliverable D4.1
950 Guidelines for performance and consequences assessment of single-site, high-risk, non-nuclear critical
951 infrastructures exposed to multiple natural hazards. STREST project: Harmonized approach to stress tests for critical
952 infrastructures against natural hazards; 2015
953 Selva J, Iqbal SM, Taroni M, Marzocchi W, Cotton F, Courage W, Abspoel-Bukman L, Miraglia S, Mignan A, Pitilakis
954 K, Argyroudis S, Kakderi K, Pitilakis D, Tsinidis G, Smerzini C. Deliverable D3.1: Report on the effects of
955 epistemic uncertainties on the definition of LP-HC events. EU FP7 research project No 603389: STREST; 2015.
956 Selva J, Tonini R, Romano F, Volpe M, Brizuela B, Piatanesi A, Basili R, Lorito S. From regional to site specific
957 SPTHA through inundation simulations: a case study for three test sites in Central Mediterranean. EGU General
958 Assembly; Vienna, Austria; 17-22 April 2016b; Abstract #EGU2016-16988.
959 Selva J, Tonini R, Molinari I, Tiberti MM, Romano F, Grezio A, Melini D, Piatanesi A, Basili R, Lorito S.
960 Quantification of source uncertainties in Seismic Probabilistic Tsunami Hazard Analysis (SPTHA). Geophys J Int
961 2016a; doi:10.1093/gji/ggw107.
962 Selva J. Long-term multi-risk assessment: statistical treatment of interaction among risks. Nat Hazards 2013; 67(2):701-
963 722.
964 Shafieezadeh A, Burden LI. Scenario-based resilience assessment framework for critical infrastructure systems: Case
965 study for seismic resilience of seaports. Reliab Eng Syst Saf 2014; 132:207-219.
966 Silva V, Crowley H, Bazzuro P. Risk-targeted hazard maps for Europe. In: Proceedings of the 2nd European Conference
967 on Earthquake Engineering and Seismology. Istanbul, Turkey; 24-29 August, 2014.

968 Smerzini C, Pitilakis K, Hasmemi K. Evaluation of earthquake ground motion and site effects in the Thessaloniki urban
969 area by 3D finite-fault numerical simulations. B Earthq Eng 2016; 15(3):787–812.
970 SRMLIFE. Development of a global methodology for the vulnerability assessment and risk management of lifelines,
971 infrastructures and critical facilities. Application to the metropolitan area of Thessaloniki. Research project, General
972 Secretariat for Research and Technology, Greece (in greek), 2007.
973 Stojadinovic B, Esposito S, Babič A, Cotton F, Dolšek M, Giardini D, Iqbal S, Mignan A, Selva J, Tsionis G. Reference
974 Report RR4: Guidelines for stress-test design for non-nuclear critical infrastructures and systems: Methodology. EU
975 FP7 research project No 603389: STREST; EUR 28342 EN, 2016; doi:10.2788/659118
976 TCLEE. Report of the 11 March 2011 Mw 9.0 Tohoku, Japan, earthquake and tsunami. Technical Council on Lifeline
977 Earthquake Engineering; 2012.
978 Toro GR. Probablistic models of site velocity profiles for generic and site-specific ground-motion amplification studies.
979 Upton, New York: Brookhaven National Laboratory, 1995.
980 Tsinker GP. Port Engineering: Planning, Construction, Maintenance, and Security, John Wiley & Sons, Inc., Hoboken,
981 New Jersey, ISBN: 978-0-471-41274-8, 2004.
982 UNCTAD. Review of Maritime Transport. In: Proceedings of the United Nations Conference on Trade and
983 Development. United Nations Publication, ISBN 978-92-1-112904-5, New York and Geneva; 2016.
984 UPGRADE. Technical reports with the calculation results of the vulnerability of specific Greek port facilities (in
985 Greek). Deliverable 8.2. Research project: Contemporary Evaluation Methodology of Seismic Vulnerability and
986 Upgrade of Port Facilities; http://excellence.minedu.gov.gr/thales/en/thalesprojects/380174, 2015.
987 Wachter J, Babeyko A, Fleischer J, Haner R, Hammitzsch M, Kloth A, Lendholt M. Development of tsunami early
988 warning systems and future challenges. Nat Hazards Earth Syst Sci 2012; 12:1923-1935.
989 Weatherill G, Esposito S, Iervolino I, Franchin P, Cavalieri F. Framework for seismic hazard analysis of spatially
990 distributed systems, in: K. Pitilakis et al. (eds). Systemic seismic vulnerability and risk assessment of complex
991 urban, utility, lifeline systems and critical facilities. Methodology and applications. Netherlands, Springer, 2014, p.
992 57-88.
993 Werner S, Taylor C. Final Report: Seismic-risk-reduction planning evaluations for wharf and embankment
994 strengthening program (WESP), Port of Oakland, Oakland CA, prepared by SEISEC-NHMI for Port of Oakland,
995 Oakland, CA, 2004.
996 Yang Z. Numerical Modeling of Earthquake Site Response Including Dilation and Liquefaction. Ph.D. Dissertation;
997 Dept. of Civil Engineering and Engineering Mechanics, Columbia University; New York, NY; 2000.
998